antioxidants

MDPI

Article

Selective HDAC8 Inhibition Attenuates Medial Vascular Calcification and Suppresses NOX2/ROS–AKT and PTEN-Associated Apoptotic Signaling

Hongyan Zhou [1], Hae Jin Kee [1,2,*], Le Wan [3], Seung Hun Lee [4], Seong Hoon Kim [4,5], Myung Ho Jeong [6] and Young Joon Hong [4,*]

[1] Heart Research Center of Chonnam National University Hospital, Gwangju 61469, Republic of Korea; zhouhy202111@gmail.com
[2] Biomedical Research Institute, Chonnam National University Hospital, Gwangju 61469, Republic of Korea
[3] Department of Orthopedics, Chonnam National University Hospital, Gwangju 61469, Republic of Korea; wle202302@gmail.com
[4] Department of Cardiology, Chonnam National University Medical School, Gwangju 61469, Republic of Korea; ish8602@naver.com (S.H.L.); kimtae1998@naver.com (S.H.K.)
[5] Department of Biomedical Sciences, Graduate School, Chonnam National University, Hwasun 58128, Republic of Korea
[6] Gwangju Veterans Hospital, Gwangju 62284, Republic of Korea; myungho6243@naver.com
* Correspondence: dg00915@cnuh.com or sshjkee@empas.com (H.J.K.); youngjoonhong@jnu.ac.kr or hyj200@hanmail.net (Y.J.H.); Tel.: +82-62-220-5823 (H.J.K.); +82-62-220-5778 (Y.J.H.); Fax: +82-62-228-4227 (H.J.K.); +82-62-223-3105 (Y.J.H.)

Abstract

Medial vascular calcification involves osteogenic reprogramming and apoptosis of vascular smooth muscle cells (VSMCs). We investigated whether histone deacetylase 8 (HDAC8) regulates oxidative and apoptotic signaling during calcification. Primary rat VSMCs were exposed to calcifying medium, and arterial calcification was induced with vitamin D_3 in mice. HDAC8 was pharmacologically inhibited with PCI-34051 and genetically modulated by knockdown or overexpression; human VSMC transcriptomes (GSE37558) were analyzed. Calcifying conditions increased HDAC8 expression, calcium deposition, and osteogenic markers. PCI-34051 and *Hdac8* knockdown attenuated calcification and osteogenic reprogramming, whereas *Hdac8* overexpression increased osteogenic markers. HDAC8 inhibition reduced NOX2 expression, reactive oxygen species, and AKT phosphorylation. PCI-34051 suppressed PTEN upregulation, caspase-8/3 and PARP1 cleavage, and apoptosis; PTEN knockdown reduced caspase-8 and caspase-3 cleavage. *Hdac8* knockdown decreased apoptosis, whereas overexpression enhanced PTEN-associated apoptotic signaling. In vitamin D_3-treated mice, PCI-34051 reduced aortic calcification, osteogenic markers, NOX2–AKT signaling, and apoptosis. Human transcriptomic analysis revealed changes associated with oxidative stress, extracellular matrix remodeling, VSMC phenotypic modulation, and programmed cell death. These findings implicate HDAC8 in calcification-associated oxidative and apoptotic injury and suggest its potential as a therapeutic target.

Keywords: vascular calcification; HDAC8; PCI-34051; oxidative stress; PTEN; apoptosis

Check for updates

Academic Editor: Antigone Lazou

Received: 16 October 2026
Revised: 16 November 2026
Accepted: 23 November 2026
Published: 28 November 2026

Copyright: © 2026 by the authors. Licensee MDPI, Basel, Switzerland. This article is an open access article distributed under the terms and conditions of the Creative Commons Attribution (CC BY) license.

1. Introduction

Vascular calcification (VC) is an actively regulated pathological process characterized by ectopic hydroxyapatite deposition in the arterial wall and is highly prevalent in hypertension, diabetes, chronic kidney disease (CKD), and advanced atherosclerosis. VC

increases arterial stiffness, impairs vascular compliance, and predicts adverse cardiovascular outcomes [1–5]. VC can be broadly categorized into intimal calcification associated with atherosclerotic plaques and medial arterial calcification (MAC, Mönckeberg's sclerosis), which preferentially involves elastic lamellae of medium-to-large arteries and is particularly common in diabetes and CKD [6,7].

A central driver of MAC is phenotypic switching of vascular smooth muscle cells (VSMCs) from a contractile state toward an osteogenic-like program, marked by induction of RUNX2, BMP2, and MSX2 together with matrix remodeling and mineral deposition. In parallel, VSMC injury and apoptosis contribute to calcification by generating membrane fragments and apoptotic bodies that can nucleate calcium phosphate deposition [5,8,9]. Despite major advances, how upstream signals integrate oxidative remodeling with cell-fate injury programs during medial calcification remains incompletely defined.

Oxidative signaling is a key determinant of VSMC reprogramming during calcification [10–13]. Reactive oxygen species (ROS), produced largely by vascular NADPH oxidases, promote osteogenic gene expression and activate AKT signaling, thereby facilitating mineralization [10–12,14]. ROS can exert biphasic effects: moderate oxidative stress may support adaptive remodeling, whereas excessive or sustained ROS can trigger cell-death cascades, exacerbating medial injury and potentially amplifying calcification via apoptotic debris [15–17]. Among NADPH oxidase isoforms, NOX2 is a prominent inducible ROS source in vascular injury and has been implicated in calcific cardiovascular settings [18]. Whether an upstream epigenetic regulator couples NOX2-associated oxidative signaling and AKT activation to apoptotic injury during MAC remains unknown.

Histone deacetylases (HDACs) regulate chromatin accessibility and non-histone signaling and influence VSMC phenotype in an isoform- and context-dependent manner [19–25]. HDAC8 is a structurally distinct class I HDAC expressed in vascular tissues and implicated in stress and remodeling. We previously reported that selective HDAC8 inhibition with PCI-34051 ameliorates cardiac and vascular remodeling in experimental heart failure and hypertension [26,27]. However, the role of HDAC8 in medial vascular calcification—and its potential to coordinate oxidative signaling and apoptosis—has not been directly tested.

Phosphatase and tensin homolog (PTEN) is widely recognized as a stress-responsive regulator of cell survival and apoptosis [28–32]. PTEN-associated apoptotic signaling may contribute to medial calcification through VSMC injury and the formation of apoptotic bodies. Previous studies have shown that apoptosis can precede VSMC calcification and that VSMC-derived apoptotic bodies can act as nucleating structures for calcium phosphate crystal deposition, thereby facilitating vascular mineralization [33]. However, whether PTEN participates in HDAC8-associated apoptotic signaling during medial calcification, and how this response relates to concurrent osteogenic remodeling, remains unclear.

Here, we tested the hypothesis that HDAC8 functions as an upstream regulator of medial vascular calcification by modulating two complementary pro-calcific processes: NOX2/ROS–AKT-associated oxidative stress and osteogenic remodeling, and PTEN-associated caspase activation and PARP1 cleavage linked to apoptotic injury. To test this hypothesis, we used calcifying VSMCs, a vitamin D_3-induced mouse model of medial calcification, pharmacological HDAC8 inhibition with PCI-34051, siRNA-mediated PTEN knockdown, and *Hdac8* gain- and loss-of-function approaches. In addition, publicly available human VSMC transcriptomic data were analyzed to provide complementary insights into calcification-associated transcriptional remodeling.

2. Materials and Methods

2.1. Reagents and Antibodies

PCI-34051 was obtained from Cayman Chemical (Ann Arbor, MI, USA). GSK2795039 (Cat. No. SML2770), N-acetyl-L-cysteine (NAC; Cat. No. A9165), silver nitrate ($AgNO_3$; Cat. No. 209139), cholecalciferol (vitamin D3; Cat. No. C9756), dimethyl sulfoxide (DMSO; Cat. No. D2650), D-(+)-glucose (Cat. No. G7528), and Kolliphor® EL (Cat. No. C5135) were purchased from Sigma-Aldrich (St. Louis, MO, USA). Dihydroethidium (DHE; Cat. No. D1168) and ProLong™ Gold Antifade Mountant with DAPI (Cat. No. P36931) were obtained from Thermo Fisher Scientific (Waltham, MA, USA). Alizarin Red S staining solution (2%; Cat. No. BA054) was purchased from BioSolution (Suwon, Republic of Korea).

The following primary antibodies were used for Western blot analysis: anti-PTEN (9552), anti-AKT (9272), anti-phospho-AKT (Ser473; 12694), anti-caspase-3 (9662), anti-caspase-8 (4790), and anti-phospho-p44/42 MAPK (ERK1/2) (Thr202/Tyr204; 4370), all from Cell Signaling Technology (Danvers, MA, USA); anti-HDAC8 (sc-374180), anti-BMP-2/4 (sc-137087), anti-MSX2 (sc-365232), anti-RUNX2 (sc-390351), anti-ERK1 (G-8; sc-271269), and anti-β-actin (sc-47778), all from Santa Cruz Biotechnology (Dallas, TX, USA); and anti-NOX2 (ab106940; Abcam, Cambridge, UK). Antibodies were used at the manufacturer-recommended dilutions. The TOPview™ Prestained Protein Ladder Marker (3.5–240 kDa; Enzynomics, Daejeon, Republic of Korea; Cat. No. EOP001S) was used as the molecular weight marker.

2.2. Plasmids and Sirnas

The plasmids used for HDAC8 overexpression included the pcDNA3.1-V5-His-TOPO empty vector and a rat *Hdac8* expression plasmid, pcDNA3.1-rat *Hdac8*-V5-TOPO. The pcDNA3.1-V5-His-TOPO vector was obtained from Invitrogen/Thermo Fisher Scientific (Waltham, MA, USA), and the rat *Hdac8* expression plasmid was generated by cloning rat *Hdac8* cDNA into this vector backbone. The *Pten*-targeting siRNA was obtained from Bioneer (Daejeon, Republic of Korea; siRNA No. 1732503), and the *Hdac8*-targeting siRNA was purchased from Dharmacon/Horizon Discovery (Cat. No. L-096589-02-0010). A negative control siRNA was purchased from Bioneer (Daejeon, Republic of Korea; Cat. No. SN-1013).

2.3. Cell Cultures

Primary vascular smooth muscle cells (VSMCs) were isolated from the thoracic aorta of male Sprague–Dawley rats (250 ± 50 g). After removing connective tissue, adventitia, and endothelium, the medial layer was minced and digested with trypsin at 37 °C. The resulting cell suspension was centrifuged, resuspended, and cultured in Dulbecco's modified Eagle's medium (DMEM) supplemented with 10% fetal bovine serum and 1% penicillin–streptomycin in a humidified incubator (37 °C, 5% CO_2). VSMCs between passages 6 and 8 were used for all experiments.

2.4. Cell Viability

Cell viability was assessed using an MTT assay. VSMCs were seeded in 96-well plates and treated with PCI-34051 (0–10 μM) for 48 h under normal growth conditions. MTT solution (0.5 mg/mL) was added for 2 h at 37 °C, after which the medium was removed, and formazan crystals were dissolved in dimethyl sulfoxide (DMSO). Absorbance was measured at 570 nm using a microplate reader, and viability was expressed as a percentage of untreated controls.

2.5. VSMC Calcification and Calcium Assay

To induce calcification in vitro, confluent VSMCs were switched from growth medium (GM) to calcification medium (CM; DMEM supplemented with 6 mM inorganic phosphate and 50 μg/mL ascorbic acid) and maintained for 4 days for qRT-PCR and Western blot analyses. For pharmacological intervention, PCI-34051 (0.1 μM) was added during the final 24 h of CM exposure.

For quantification of calcium deposition, VSMCs were seeded in 12-well plates and cultured in CM for 6 days, with PCI-34051 (1 μM) added during the final 3 days where indicated. At the end of the incubation, cells were washed twice with PBS and decalcified with 0.6 N HCl overnight at 4 °C. The HCl supernatant was collected, and calcium content was measured colorimetrically at 620 nm using a commercial assay kit (QuantiChrom™ Calcium Assay Kit; BioAssay Systems, Hayward, CA, USA). The remaining cell layer was solubilized in 0.1 N NaOH containing 0.1% SDS for protein quantification, and calcium levels were expressed as μg Ca^{2+} per mg protein. For tissue samples, calcium content was normalized to wet tissue weight.

2.6. Transfection

For siRNA-mediated knockdown, rat aortic vascular smooth muscle cells were transfected with siRNAs targeting *Pten* or *Hdac8*, or with negative control siRNA, at a final concentration of 100 nM using Lipofectamine™ RNAiMAX reagent (Thermo Fisher Scientific, Waltham, MA, USA) according to the manufacturer's instructions. After 48 h of transfection, cells were harvested for subsequent analyses or switched to CM for an additional 4 days, with medium changes every 2 days.

The rat A10 vascular smooth muscle cell line (ATCC CRL-1476) was obtained from the American Type Culture Collection (ATCC, Manassas, VA, USA). A10 cells were cultured under standard conditions and used for HDAC8 overexpression experiments. For HDAC8 overexpression, A10 cells were transfected with either the pcDNA3.1-V5-His-TOPO empty vector or the pcDNA3.1-rat *Hdac8*-V5-TOPO expression plasmid using Lipofectamine™ 3000 reagent (Thermo Fisher Scientific) according to the manufacturer's instructions. For qRT-PCR experiments, cells were transfected with 1 μg of plasmid DNA per well in 12-well plates, whereas for Western blot analysis, cells were transfected with 2 μg of plasmid DNA per well in 6-well plates. After 48 h of transfection, cells were harvested for subsequent analyses.

2.7. In Vitro Calcification Staining (Alizarin Red S)

To assess in vitro calcium deposition, rat aortic VSMCs were subjected to calcifying conditions. For HDAC8 inhibition experiments, cells were cultured in GM or CM for 6 days, with PCI-34051 (1 μM) or vehicle administered during the final 3 days. For knockdown studies, VSMCs were transfected with siRNA targeting Hdac8 or Pten, or negative control siRNA (siControl; 100 nM), for 48 h before switching to GM or CM for an additional 4 days. At the end of treatment, cells were washed twice with PBS and fixed in 1.85% paraformaldehyde for 15 min at room temperature. Fixed cultures were stained with 2% Alizarin Red S solution (pH 4.2) for 15 min and then washed repeatedly with deionized water to remove excess dye. Plates were air-dried, and mineral deposition was visualized using an inverted light microscope (Nikon, Japan).

2.8. DHE Staining for Intracellular ROS

Intracellular ROS generation was assessed using the superoxide-sensitive fluorescent probe dihydroethidium (DHE). For HDAC8 inhibition experiments, VSMCs were cultured in GM or CM for 4 days, with PCI-34051 (0.1 μM) or vehicle administered during the final 24 h.

For HDAC8 knockdown experiments, VSMCs were transfected with siRNA targeting *Hdac8* or negative control siRNA (siControl; 100 nM) for 48 h and then maintained in GM or CM for an additional 4 days before DHE staining. For HDAC8 overexpression and antioxidant rescue experiments, A10 cells were transfected with either an empty vector or a rat *Hdac8* expression plasmid (1 μg/well in 12-well plates) using Lipofectamine™ 3000 reagent. After 48 h, cells were pretreated with NAC (1 mM) or vehicle for 3 h and subsequently cultured in GM or CM for 6 h prior to DHE staining.

For the NOX2 inhibition experiment, VSMCs were seeded and allowed to attach overnight. The following day, cells were pretreated with GSK2795039, a selective NOX2 inhibitor, at 20 μM or with DMSO vehicle for 1 h. The medium was then replaced with GM or CM containing GSK2795039 or DMSO vehicle, and cells were cultured for an additional 24 h before DHE staining.

After the indicated treatments, cells were washed with warm PBS and incubated with DHE solution (5 μM in serum-free medium) for 15 min at 37 °C in the dark. Cells were then washed with PBS, mounted with DAPI-containing mounting medium, and imaged immediately. For the PCI-34051, siRNA-mediated *Hdac8* knockdown, and HDAC8 overexpression/NAC experiments, DHE fluorescence was detected using a TRITC filter set (excitation: 540/25 nm; dichroic mirror: 565 nm; emission: 605/55 nm) on a Nikon Eclipse 80i fluorescence microscope (Nikon, Tokyo, Japan). For the GSK2795039 experiment, fluorescence images were acquired using a laser scanning confocal microscope (LSM 510; Carl Zeiss, Oberkochen, Germany), with DHE fluorescence captured in the red channel and DAPI nuclear staining captured in the blue channel. All images within the same experiment were acquired under identical exposure and imaging settings. DHE fluorescence intensity was quantified using ImageJ software (version 1.53t; National Institutes of Health, Bethesda, MD, USA) by measuring the mean fluorescence intensity per field and normalizing the values to the corresponding control group.

2.9. TUNEL Staining in Cultured VSMCs

Apoptotic DNA fragmentation was evaluated using the DeadEnd™ Fluorometric TUNEL System (G3250; Promega, Madison, WI, USA) according to the manufacturer's protocol for adherent cells. VSMCs grown on coverslips were used for TUNEL staining. For the HDAC8 inhibition experiment, cells were cultured in GM or CM for 4 days, with PCI-34051 (0.1 μM) or vehicle administered during the final 24 h. For the HDAC8 knockdown experiment, VSMCs were transfected with siRNA targeting *Hdac8* or negative control siRNA (siControl) for 48 h. After transfection, cells were switched to GM or CM and maintained for an additional 4 days, with medium changes every 2 days. After the indicated treatments, cells were fixed with 4% formaldehyde in PBS for 25 min at 4 °C, washed twice with PBS, and permeabilized with 0.2% Triton X-100 for 5 min. Following two additional PBS washes, cells were equilibrated with Equilibration Buffer for 10 min at room temperature and then incubated with the TdT reaction mixture for 60 min at 37 °C in the dark. The reaction was terminated with 2× SSC for 15 min. Slides were then washed with PBS, mounted with DAPI-containing mounting medium, and imaged immediately by fluorescence microscopy.

TUNEL-positive nuclei were visualized as green fluorescence, and total nuclei were identified by DAPI staining. Images within the same experiment were acquired under identical imaging settings. TUNEL-positive cells were quantified using ImageJ software and expressed as the percentage of TUNEL-positive nuclei among total DAPI-stained nuclei. Where indicated, values were normalized to the corresponding control group.

2.10. In Vivo Vitamin D_3-Induced Medial Calcification Model and Tissue Collection

All animal experiments were approved by the Institutional Animal Care and Use Committee of Chonnam National University Medical School (CNUH IACUC-22023; approved on 26 September 2022) and were conducted in accordance with institutional guidelines, the ARRIVE guidelines 2.0, and the Guide for the Care and Use of Laboratory Animals (US National Institutes of Health Publications, 8th edition, 2011). Eight-week-old male C57BL/6N mice (21–24 g) were housed under controlled conditions with free access to food and water. Mice were randomly assigned to three groups: control, vitamin D_3, and vitamin D_3 + PC-I34051. Investigators performing histological and molecular analyses were blinded to group allocation.

Medial aortic calcification was induced by subcutaneous administration of vitamin D_3 at 400,000 IU/kg/day for 5 consecutive days. The vitamin D_3 dosing regimen was selected based on previously established protocols for reproducible induction of medial vascular calcification in mice [34,35]. The vitamin D_3 solution was prepared using a modified solubilization procedure. Briefly, cholecalciferol was first dissolved in DMSO, followed by the addition of Kolliphor® EL as a solubilizing agent. D-(+)-glucose dissolved in sterile distilled water was then added to the cholecalciferol mixture, and the final solution was thoroughly mixed before subcutaneous injection [36,37]. The corresponding vehicle was prepared using the same formulation without cholecalciferol. Mice in the treatment group received PCI-34051 at 3 mg/kg/day by intraperitoneal injection once daily for 7 days, starting on day 2 after the first vitamin D_3 injection. The dose and treatment schedule of PCI-34051 were selected based on previous studies evaluating selective HDAC8 inhibition in vivo [27]. Control mice received the corresponding vehicle. Body weight and general health status were monitored throughout the experiment. Animals were euthanized on day 9.

At the experimental endpoint, the whole aorta, including the aortic arch, thoracic aorta, and abdominal aorta, was carefully dissected and immediately placed in ice-cold PBS. Surrounding adipose and connective tissues were removed under a stereomicroscope. Aortic tissues were then allocated for histological staining, calcium quantification, RNA extraction, and protein analysis. For histological analyses, aortic tissues were fixed in 3.7% formaldehyde, dehydrated, embedded in paraffin, and sectioned at 5 µm. Serial sections were used for H&E, Alizarin Red S, von Kossa, and TUNEL staining. Remaining aortic tissues were snap-frozen in liquid nitrogen and stored at −80 °C for subsequent RNA and protein analyses.

2.11. Histology, Calcification Staining, and TUNEL Analysis of Aortic Tissue

2.11.1. Hematoxylin and Eosin Staining

Paraffin-embedded aortic arch tissues were sectioned at a thickness of 5 µm. Sections were deparaffinized in xylene, rehydrated through a graded ethanol series, and rinsed in distilled water. For hematoxylin and eosin staining, sections were stained with hematoxylin for approximately 4 min, rinsed under running tap water for 5 min, and counterstained with eosin for 1 min. After dehydration and clearing in xylene, sections were mounted and observed under a Nikon Eclipse 80i microscope. Aortic medial morphology, wall thickness, and elastic lamellar integrity were evaluated.

2.11.2. Alizarin Red S Staining

To detect calcium deposition, deparaffinized and rehydrated aortic sections were rinsed with distilled water and incubated with 2% Alizarin Red S solution at pH 4.2 for approximately 1 min until red-orange calcium deposits became visible. Excess dye was removed by gentle washing. Sections were dehydrated in acetone, cleared sequentially in acetone–xylene and xylene, and mounted for microscopic observation.

2.11.3. Von Kossa Staining

For von Kossa staining, deparaffinized and rehydrated sections were rinsed thoroughly with distilled water and incubated with 5% silver nitrate solution under ultraviolet light for 60 min until calcium phosphate deposits appeared black or dark brown. Residual silver nitrate was removed by washing with distilled water. Sections were counterstained with eosin for 1 min, dehydrated through graded ethanol, cleared in xylene, and mounted for microscopic evaluation.

2.11.4. TUNEL Staining

Apoptosis in aortic tissue was evaluated using the DeadEnd™ Fluorometric TUNEL System (Promega, Madison, WI, USA) according to the manufacturer's protocol for paraffin-embedded tissues with minor modifications. Briefly, paraffin sections were deparaffinized, rehydrated, and incubated sequentially in 0.85% NaCl and PBS. Sections were fixed with 4% formaldehyde for 15 min and permeabilized with proteinase K at 20 µg/mL for 10 min. After equilibration, sections were incubated with the TdT reaction mixture for 60 min at 37 °C in the dark. The reaction was terminated with 2× SSC, followed by PBS washes. Slides were mounted with DAPI-containing mounting medium and imaged by fluorescence microscopy.

TUNEL-positive nuclei were visualized as green fluorescence, and total nuclei were identified by DAPI staining. Images within the same experiment were acquired under identical imaging settings. TUNEL-positive signals were quantified using ImageJ software and expressed as TUNEL-positive area relative to total vessel area, or as the percentage of TUNEL-positive nuclei among total DAPI-stained nuclei.

2.12. Quantitative Reverse Transcription PCR Analysis

Total RNA was extracted from cultured VSMCs, A10 cells, and mouse aortic tissues using TRIzol™ reagent (Invitrogen, Carlsbad, CA, USA) according to the manufacturer's instructions. RNA concentration and purity were assessed spectrophotometrically by measuring absorbance at 260 and 280 nm using an ACTGene ASP-2680 spectrophotometer (Piscataway, NJ, USA). RNA samples with an A260/A280 ratio of 1.8–2.0 were used for subsequent analysis.

Complementary DNA (cDNA) was synthesized from 1 µg of total RNA using TOPscript™ RT DryMIX (Enzynomics, Daejeon, Republic of Korea) in a 20 µL reaction volume. Quantitative real-time PCR was performed using SYBR® Green PCR Master Mix (Applied Biosystems, Foster City, CA, USA) and gene-specific primers in 20 µL reactions. Relative mRNA expression levels were calculated using the $2^{-\Delta\Delta Ct}$ method and normalized to *Gapdh* or *Actb*, as appropriate for each experiment. Data are presented as fold changes relative to the corresponding control group. All reactions were performed in technical triplicates. Primer sequences used for qRT-PCR are listed in Table 1.

2.13. Western Blotting

Total protein was extracted from cultured cells and mouse aortic tissues using ice-cold RIPA lysis buffer supplemented with protease and phosphatase inhibitors. For aortic protein extraction, frozen thoracic and abdominal aortas were minced on ice, lysed in RIPA buffer, and mechanically homogenized. Lysates were incubated on ice for 30 min with intermittent mixing and centrifuged at 12,000× *g* for 15 min at 4 °C. The supernatants were collected, and protein concentrations were determined using a bicinchoninic acid protein assay kit (Pierce, Rockford, IL, USA).

Table 1. Primers used in quantitative real-time polymerase chain reaction analysis.

Genes	Primer Sequence (5′ to 3′)
Gapdh (rat_NM_017008.5)	F: AACCCATCACCATCTTCCAGGAGC R: ATGGACTGTGGTCATGAGCCCTTC
Bmp2 (rat_NM_017178.2)	F: TACCCCCGGCTGTGATGCGA R: ACCCGCAACCCTCCACAACC
Runx2 (rat_NM_001278483.2)	F: GAGCACAAACATGGCTGAGA R: TGGAGATGTTGCTCTGTTCG
Msx2 (rat_NM_012982.3)	F: AACACAAGACCAACCGGAAG R: GCAGCCATTTTCAGCTTTTC
Nox1 (rat_NM_053683.2)	F: AGCCATTGGATCACAACCTC R: TGGATGGGATTTAGCCAAGA
Nox2 (Cybb_rat_NM_023965.2)	F: TGTCATTCTGGTGTGGTTGG R: GAACCCCTGAGGAAGGAGAG
Nox4 (rat_NM_053524.1)	F: CTGGAAGAACCCAAGTTCCA R: ACTGGCCAGGTCTTGCTTTA
Pten (rat_NM_031606.2)	F: TGACACCGCCAAATTTAACTGCAG R: TCCGCCACTGAACATTGGAATAGT
Hdac1 (rat_NM_001025409.1)	F: AGGGCACCAAGAGGAAAGTCTGTT R: TTCAGACTTCTTCGCATGGTGCAG
Hdac2 (rat_NM_053447.2)	F: CTGCACCACGCCAAGAAGTCAGA R: CAGTTAGGTTGAAGCAGCCCAGCC
Hdac3 (rat_NM_053448.2)	F: CAAGACCGTGGCGTATTTCTACGA R: GCCCAGTTGATGGCAATATCACAG
Hdac8 (rat_NM_001126373.2)	F: CGCTACCCCCGGTTTATATT R: CTTCTTGGCTGACCTTCTGG
Gapdh (mouse_NM_001411840.1)	F: GGGTCCCAGCTTAGGTTCAT R: CATTCTCGGCCTTGACTGTG
Bmp2 (mouse_NM_007553.3)	F: TCCCCAGTGACGAGTTTCTC R: CGAAGCTCTCCCACTGACTT
Runx2 (mouse_NM_001145920.3)	F: GCCCAGGCGTATTTCAGATG R: GGTAAAGGTGGCTGGGTAGT
Msx2 (mouse_NM_013601.2)	F: TTCACCACATCCCAGCTTCT R: TTCAGCTTTTCCAGTTCCGC
Hdac8 (mouse_NM_001313742.1)	F: ATCAACTGGTCTGGAGGGTG R: CATGTCACCTGTTCCTGGGA
Actb (mouse_NM_007393.5)	F: CCTCTATGCCAACACAGTGC R: CCTGCTTGCTGATCCACATC

Equal amounts of protein (30 μg per lane) were mixed with 4× Laemmli sample buffer, denatured at 95 °C for 5 min, separated by SDS-PAGE, and transferred onto PVDF membranes (Millipore, Billerica, MA, USA). Molecular weights were estimated using prestained protein markers. Membranes were blocked with 5% nonfat dry milk or 5% bovine serum albumin in TBST for 1 h at room temperature and then incubated overnight at 4 °C with the indicated primary antibodies. After three washes with TBST, membranes were incubated with the appropriate HRP-conjugated secondary antibodies for 1 h at room temperature.

Protein bands were visualized using enhanced chemiluminescence substrate and imaged with an iBright FL1500 imaging system (Thermo Fisher Scientific, Waltham, MA, USA). Densitometric analysis was performed using ImageJ software. Target protein expression was normalized to β-actin, and phosphorylated proteins were normalized to their corresponding total protein levels where applicable.

2.14. External Transcriptomic Analysis of Human VSMC Osteogenic Differentiation

The public microarray dataset GSE37558 was obtained from the Gene Expression Omnibus (GEO) database. This dataset contains gene expression profiles of primary human vascular smooth muscle cells undergoing osteogenic differentiation at days 0, 2, 8, 12, and 25. Day 0 was used as the baseline reference, and day 12 was selected as a representative time point for global transcriptional analysis. Differentially expressed genes were identified using an adjusted p value of <0.05 and an absolute log2 fold change ≥1 (Supplementary Table S1). For genes represented by multiple probes, the probe with the smallest adjusted p value was selected for volcano plot analysis. Volcano plots were generated using ImageGP 2 [38], with selected genes related to oxidative stress, apoptosis, extracellular matrix remodeling, and VSMC phenotypic modulation highlighted.

For time-course heatmap analysis, log2 fold-change values of selected genes at days 2, 8, 12, and 25 relative to day 0 were extracted from GSE37558 (Supplementary Table S2). A consistent representative probe was used for each gene across all time points. Heatmaps were generated using ImageGP 2 without row-wise scaling to preserve the original log2 fold-change values.

Significantly upregulated genes at day 12 (adjusted $p < 0.05$ and log2 fold change ≥1) were subjected to GO Biological Process and Reactome enrichment analyses using Metascape (Supplementary Table S3). Enriched terms were visualized as a functional similarity network and summarized in a bubble plot generated using ImageGP 2. This dataset was used as an external human transcriptomic reference for calcification-associated molecular remodeling rather than as direct evidence of HDAC8 inhibition.

2.15. Statistical Analysis

Data are expressed as mean ± standard deviation (SD). Statistical analyses were performed using GraphPad Prism 8 (GraphPad Software, San Diego, CA, USA). Comparisons between two groups were made using unpaired t-tests, and differences among multiple groups were assessed by one-way ANOVA followed by appropriate post hoc tests. A p-value < 0.05 was considered statistically significant.

3. Results

3.1. PCI-34051 Suppresses Calcification and Osteogenic Reprogramming in VSMCs

To determine whether pharmacological inhibition of HDAC8 attenuates vascular smooth muscle cell calcification, we first examined the effect of the selective HDAC8 inhibitor PCI-34051 in cultured VSMCs. The chemical structure of PCI-34051 is shown in Figure 1A. MTT analysis demonstrated that PCI-34051 did not significantly affect VSMC viability at concentrations up to 10 μM after 48 h of treatment, supporting the use of 0.1 μM PCI-34051 for subsequent experiments (Figure 1B).

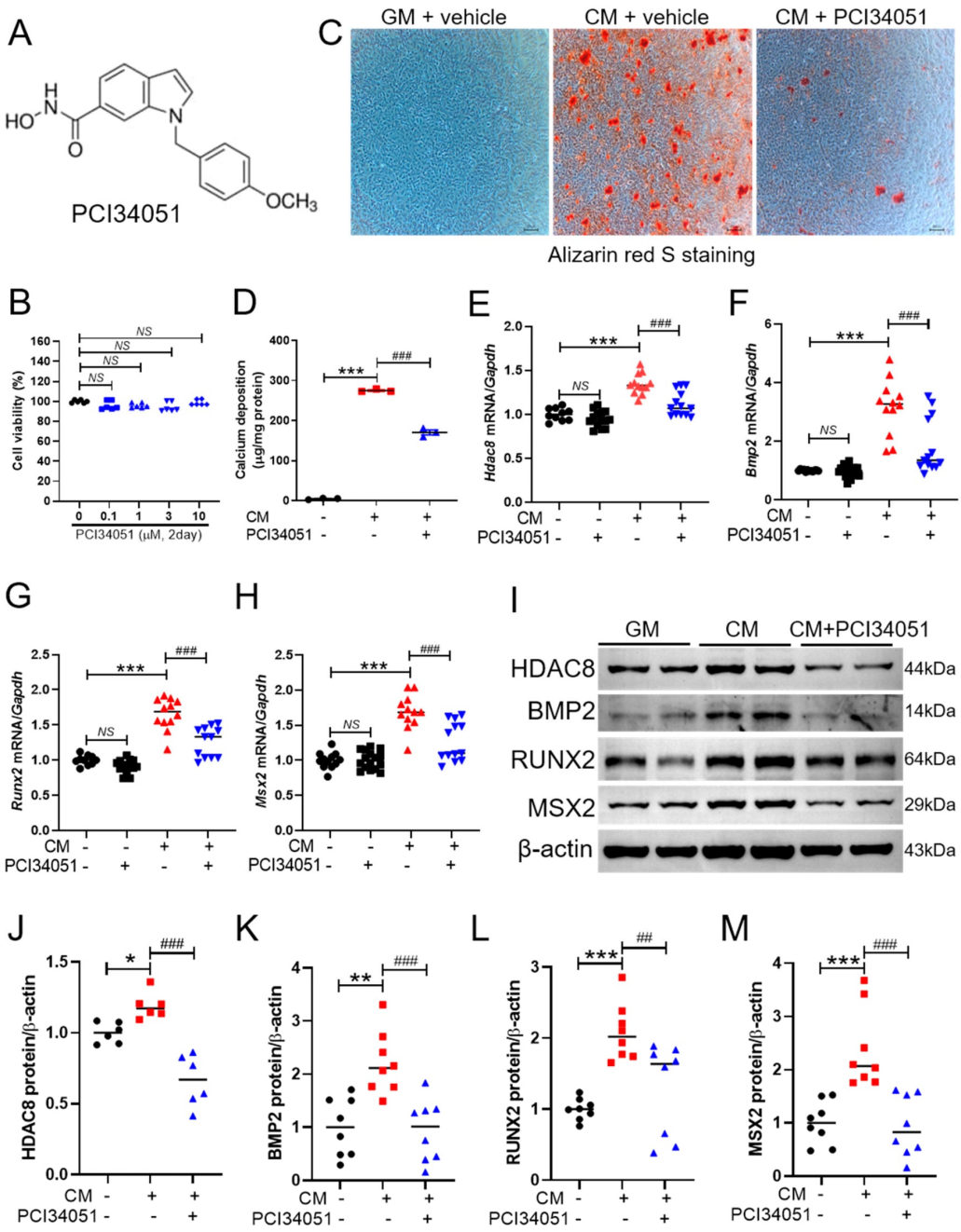


Figure 1. PCI-34051 suppresses calcification and osteogenic reprogramming in VSMCs. (**A**) Chemical structure of PCI-34051. (**B**) VSMC viability after 48 h of treatment with PCI-34051 at the indicated concentrations, assessed by the MTT assay ($n = 6$). (**C**) Representative Alizarin Red S staining of VSMCs cultured in growth medium (GM) or calcification medium (CM) for 6 days, with vehicle or PCI-34051 (1 μM) added during the final 3 days. Scale bar: 200 μm. (**D**) Quantification of calcium content under the conditions described in (**C**) ($n = 3$). (**E**–**H**) qRT-PCR analysis of *Hdac8*, *Bmp2*, *Runx2*, and *Msx2* mRNA expression in VSMCs cultured in GM or CM for 4 days, with vehicle or PCI-34051 (0.1 μM) added during the final 24 h ($n = 12$–14). (**I**) Representative Western blot images of HDAC8, BMP2, RUNX2, and MSX2 under the treatment conditions described in (**E**–**H**), with β-actin as the loading control. (**J**–**M**) Densitometric analysis of HDAC8, BMP2, RUNX2, and MSX2 protein levels normalized to β-actin ($n = 6$–8). Data are presented as mean ± SD. * $p < 0.05$, ** $p < 0.01$, *** $p < 0.001$; ## $p < 0.01$, ### $p < 0.001$; NS, not significant. GM, growth medium; CM, calcification medium. Each dot represents one independent biological experiment (not a technical replicate).

3.2. Genetic Manipulation Confirms HDAC8 as a Pro-Calcific Regulator in VSMCs

To investigate whether HDAC8 contributes to VSMC calcification, we performed loss- and gain-of-function experiments. Knockdown of *Hdac8* by siRNA significantly reduced CM-induced calcium deposition, as shown by Alizarin Red S staining and calcium quantification (Figure 2A,B). At the molecular level, efficient silencing of Hdac8 was associated with reduced CM-induced expression of the osteogenic genes *Bmp2* and *Msx2*, whereas *Runx2* expression was not significantly altered (Figure 2C–F). Western blot analysis further confirmed that HDAC8 depletion significantly reduced CM-induced BMP2 and MSX2 protein expression, whereas RUNX2 protein levels were not significantly altered (Figure 2G–K). To investigate potential compensatory changes in other class I HDACs following Hdac8 knockdown, we examined the mRNA expression of *Hdac1*, *Hdac2*, and *Hdac3*. Hdac8 knockdown significantly increased *Hdac1* mRNA expression under calcifying conditions, whereas *Hdac2* and *Hdac3* expression remained unchanged compared with the siControl + CM group (Supplementary Figure S1A–C).

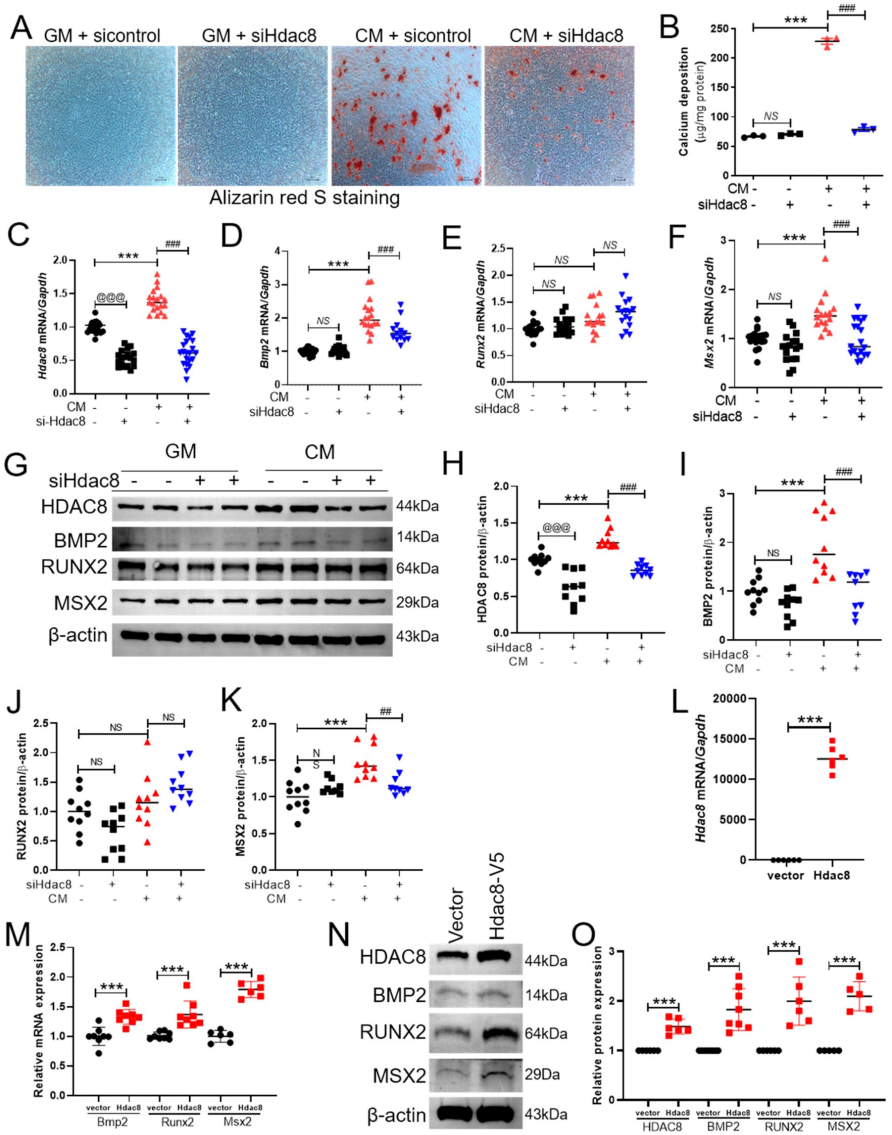


Figure 2. Genetic manipulation identifies HDAC8 as a pro-calcific regulator in VSMCs. (**A**) Representative Alizarin Red S staining of VSMCs transfected with siControl or siHdac8 for 48 h and subsequently cultured in GM or CM for 4 days. Scale bar: 200 μm. (**B**) Quantification of calcium deposition under

the conditions shown in (**A**) ($n = 3$). (**C**–**F**) qRT-PCR analysis of *Hdac8*, *Bmp2*, *Runx2*, and *Msx2* mRNA expression ($n = 13$–20). (**G**) Representative Western blot images of HDAC8, BMP2, RUNX2, and MSX2, with β-actin as the loading control. (**H**–**K**) Densitometric analysis of HDAC8, BMP2, RUNX2, and MSX2 protein levels normalized to β-actin ($n = 8$–10). A10 cells were transfected with empty vector or an *Hdac8* expression plasmid for 48 h. (**L**–**M**) qRT-PCR analysis of *Hdac8*, *Bmp2*, *Runx2*, and *Msx2* mRNA expression ($n = 6$–8). (**N**) Representative Western blot images of HDAC8, BMP2, RUNX2, and MSX2, with β-actin as the loading control. (**O**) Densitometric analysis of HDAC8, BMP2, RUNX2, and MSX2 protein levels normalized to β-actin ($n = 5$–8). Data are presented as mean ± SD. $^{@@@}$ $p < 0.001$; *** $p < 0.001$; $^{\#\#}$ $p < 0.01$, $^{\#\#\#}$ $p < 0.001$; NS, not significant. GM, growth medium; CM, calcification medium. Each dot represents one independent biological experiment (not a technical replicate).

To further determine whether HDAC8 overexpression promotes osteogenic marker expression, A10 cells were transfected with an Hdac8 expression plasmid. *Hdac8* overexpression markedly increased *Hdac8* expression and upregulated the osteogenic markers *Bmp2*, *Runx2*, and *Msx2* at the mRNA level (Figure 2L,M). Consistently, HDAC8 overexpression increased the protein abundance of BMP2, RUNX2, and MSX2 (Figure 2N,O). These gain- and loss-of-function data support a pro-calcific role for HDAC8 in VSMC osteogenic reprogramming.

3.3. HDAC8 Promotes NOX2-Associated ROS Accumulation Under Calcifying Conditions

Because oxidative stress is a key driver of VSMC calcification, we next examined whether HDAC8 regulates ROS accumulation under calcifying conditions. DHE staining showed that CM markedly increased intracellular DHE fluorescence compared with GM. PCI-34051 significantly reduced CM-induced DHE fluorescence, suggesting that HDAC8 inhibition attenuates ROS-associated oxidative responses in calcifying VSMCs (Figure 3A,B).

Consistent with the pharmacological inhibition results, *Hdac8* knockdown also decreased CM-induced DHE fluorescence in VSMCs (Figure 3C,D). Conversely, *Hdac8* overexpression enhanced DHE fluorescence in A10 cells, particularly under calcifying conditions. Pretreatment with the antioxidant NAC reduced the increase in DHE fluorescence observed following *Hdac8* overexpression, supporting the involvement of ROS in HDAC8-associated oxidative responses (Figure 3E,F). To determine whether NOX2 contributes to this ROS signal, VSMCs were treated with the NOX2 inhibitor GSK2795039. GSK2795039 significantly reduced CM-induced DHE fluorescence, indicating that NOX2 activity contributes to ROS accumulation during VSMC calcification (Figure 3G,H). These findings support a role for HDAC8 in promoting oxidative responses under calcifying conditions, with NOX2 activity contributing to CM-induced ROS accumulation.

3.4. HDAC8 Preferentially Modulates NOX2 and Is Associated with NOX2–AKT Signaling Under Calcifying Conditions

To determine whether HDAC8 preferentially regulates specific NADPH oxidase isoforms under calcifying conditions, we examined the expression of *Nox1*, *Nox2*, and *Nox4*. In VSMCs, CM increased the mRNA levels of *Nox1*, *Nox2*, and *Nox4* to varying degrees compared with GM. However, PCI-34051 selectively decreased CM-induced *Nox2* upregulation without comparably affecting *Nox1* or *Nox4* (Figure 4A–C). Consistently, under CM conditions, *Hdac8* knockdown reduced *Nox2* expression relative to siControl + CM, whereas *Nox1* and *Nox4* were not significantly altered (Figure 4D–F). Conversely, *Hdac8* overexpression in A10 cells markedly increased *Nox2* mRNA expression but did not significantly affect *Nox1* or *Nox4* (Figure 4G). Notably, under basal GM conditions, Hdac8 knockdown increased *Nox1* and decreased *Nox4* mRNA expression, indicating that HDAC8-associated regulation of NOX isoforms is context-dependent. Nevertheless, under calcifying conditions, Nox2 was

the most consistently responsive isoform to HDAC8 modulation. These findings suggest that *Nox2* is preferentially responsive to HDAC8 manipulation among the NOX isoforms examined under calcifying conditions.

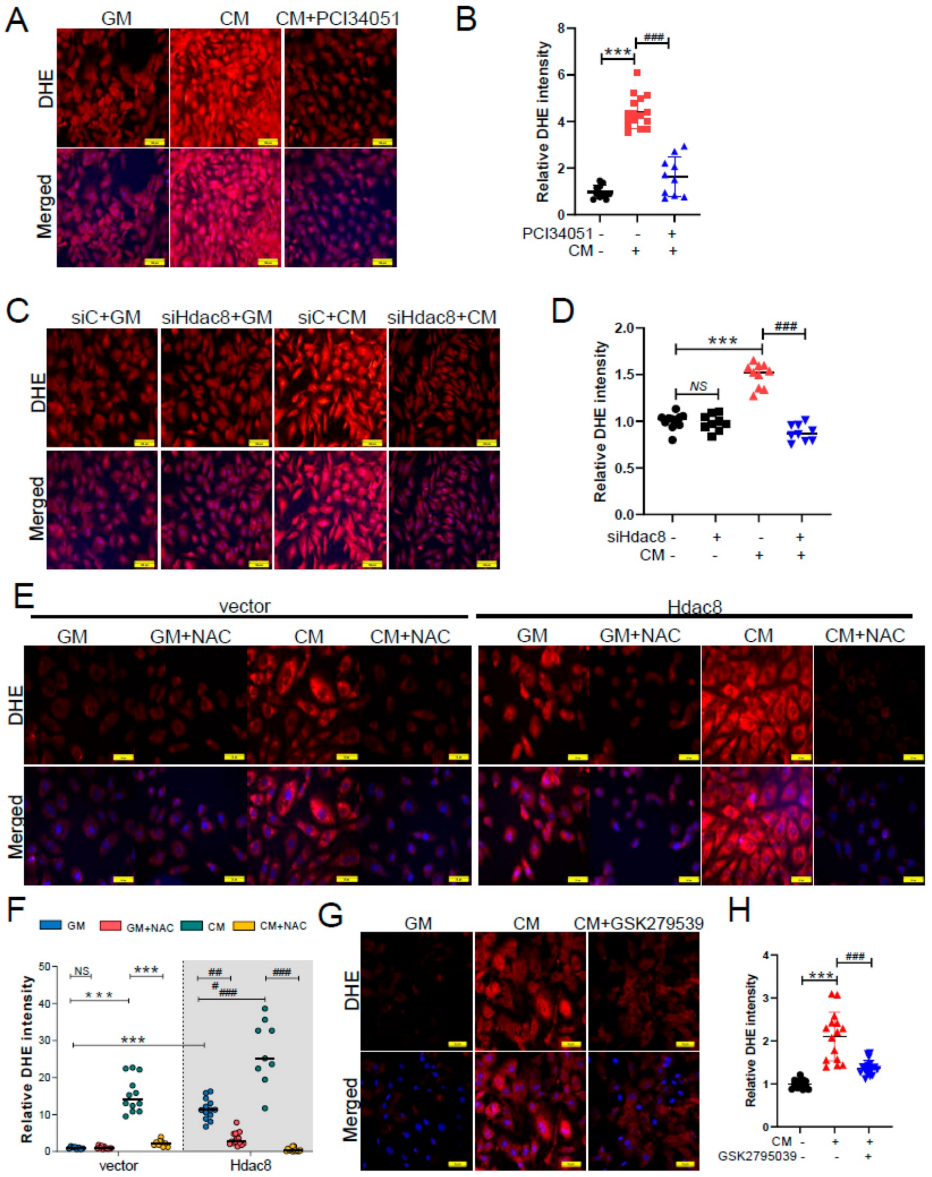


Figure 3. HDAC8 promotes NOX2-associated ROS accumulation under calcifying conditions. (**A**,**B**) Representative DHE staining images and fluorescence quantification in VSMCs cultured in GM or CM for 4 days, with vehicle or PCI-34051 (0.1 μM) added during the final 24 h (n = 10–16). Scale bar: 100 μm. (**C**,**D**) Representative DHE staining images and quantification in VSMCs transfected with siControl or siHdac8 (100 nM) for 48 h and subsequently exposed to GM or CM for 4 days (n = 9–11). Scale bar: 100 μm. (**E**,**F**) Representative DHE staining images and quantification in A10 cells transfected with empty vector or an *Hdac8* expression plasmid (1 μg) for 48 h, with or without NAC (1 mM) pretreatment for 3 h, followed by incubation in GM or CM for 6 h (n = 8–16). Scale bar: 50 μm. (**G**,**H**) Representative DHE staining images and quantification in VSMCs cultured in GM or CM for 24 h in the presence or absence of the NOX2 inhibitor GSK2795039 (20 μM). Scale bar: 50 μm. DHE fluorescence intensity was measured using ImageJ and expressed relative to the corresponding control. Data are presented as mean ± SD. *** $p < 0.001$; $^{\#}$ $p < 0.05$; $^{\#\#}$ $p < 0.01$; $^{\#\#\#}$ $p < 0.001$; NS, not significant. GM, growth medium; CM, calcification medium; NAC, N-acetylcysteine. Each dot represents the mean value from one independent experiment, calculated from multiple microscopic fields.

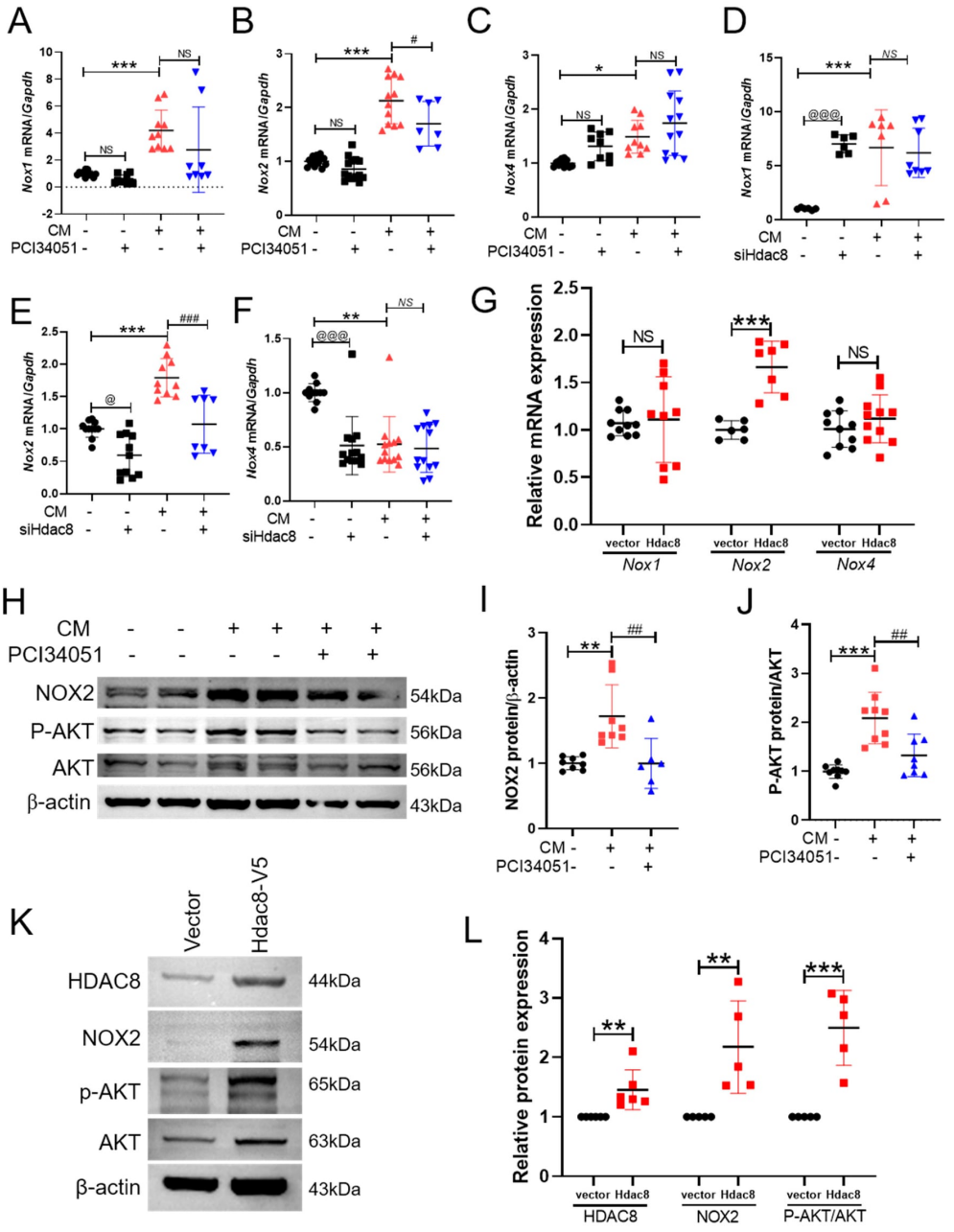


Figure 4. HDAC8 preferentially modulates NOX2 expression under calcifying conditions and is associated with AKT activation. (**A**–**C**) qRT-PCR analysis of *Nox1*, *Nox2*, and *Nox4* mRNA expression in VSMCs cultured in GM or CM for 4 days, with vehicle or PCI-34051 (0.1 μM) added during the final 24 h (n = 7–12). (**D**–**F**) qRT-PCR analysis of *Nox1*, *Nox2*, and *Nox4* mRNA expression in VSMCs transfected with siControl or siHdac8 for 48 h and subsequently cultured in GM or CM for 4 days (n = 6–13). (**G**) qRT-PCR analysis of *Nox1*, *Nox2*, and *Nox4* mRNA expression in A10 cells transfected with empty vector or an *Hdac8* expression plasmid (n = 6–12). (**H**–**J**) Representative Western blot images and densitometric quantification of NOX2, p-AKT, and total AKT in VSMCs cultured in GM or CM for 4 days, with vehicle or PCI-34051 (0.1 μM) administered during the final 24 h before cell harvest (n = 6–9). (**K**,**L**) Representative Western blot images and densitometric quantification of HDAC8, NOX2, p-AKT, and total AKT in A10 cells transfected with empty vector or Hdac8 expression plasmid for 48 h (n = 5–6). Data are presented as mean ± SD. Each dot represents one independent biological experiment. $^{@@@}$ $p < 0.001$; * $p < 0.05$; ** $p < 0.01$; *** $p < 0.001$; $^{\#}$ $p < 0.05$; $^{\#\#}$ $p < 0.01$; $^{\#\#\#}$ $p < 0.001$. NS, not significant. GM, growth medium; CM, calcification medium.

Based on these observations, we next examined the relationship between HDAC8-associated NOX2 expression and AKT activation during VSMC calcification. Western blot analysis showed that CM increased NOX2 protein expression and enhanced AKT phosphorylation, as indicated by an increased p-AKT/AKT ratio. PCI-34051 attenuated both CM-induced NOX2 upregulation and AKT phosphorylation (Figure 4H–J), suggesting that HDAC8 inhibition reduces NOX2 expression and AKT activation under calcifying conditions. In gain-of-function experiments, *Hdac8* overexpression increased HDAC8 and NOX2 protein abundance and enhanced AKT phosphorylation in A10 cells (Figure 4K,L). Collectively, these findings demonstrate that HDAC8 regulates NOX2 expression and is associated with changes in AKT phosphorylation under calcifying conditions.

3.5. PTEN Contributes to Caspase-Associated Apoptotic Signaling During VSMC Calcification

In parallel with the NOX2-associated AKT signaling, we investigated whether HDAC8 also regulates apoptosis-associated responses under calcifying conditions. Western blot analysis showed that CM increased PTEN protein expression and enhanced caspase-dependent apoptotic signaling, as evidenced by increased cleaved caspase-8/caspase-8, cleaved caspase-3/caspase-3, and cleaved PARP1/PARP1 ratios. PCI-34051 treatment significantly attenuated these CM-induced changes (Figure 5A–E). TUNEL staining further demonstrated that CM markedly increased apoptosis in VSMCs, whereas PCI-34051 reduced CM-induced TUNEL positivity (Figure 5F,G).

To determine whether PTEN contributes to caspase activation under calcifying conditions, VSMCs were transfected with siPTEN and then exposed to GM or CM. PTEN knockdown reduced PTEN protein abundance under both GM and CM conditions. Although caspase activation was not significantly altered by PTEN knockdown under GM conditions, the CM-induced increases in cleaved caspase-8/caspase-8 and cleaved caspase-3/caspase-3 ratios were significantly attenuated by PTEN knockdown (Figure 5H–K). These findings suggest that PTEN contributes to caspase activation particularly under calcifying stress.

PTEN knockdown did not suppress CM-induced *Bmp2* or *Runx2* mRNA expression and significantly increased *Msx2* mRNA expression under calcifying conditions (Figure 5L–O). Alizarin Red S staining and image-based quantification showed that CM significantly increased staining intensity in siControl-transfected VSMCs. Under CM conditions, staining intensity did not differ significantly between the siControl and siPTEN groups (Figure 5P,Q). These findings indicate that PTEN knockdown attenuates CM-induced caspase activation without significantly suppressing the osteogenic markers examined or mineral deposition. Together, these results support a role for PTEN in caspase-associated apoptotic signaling during VSMC calcification.

3.6. Genetic Modulation of HDAC8 Supports PTEN-Associated Caspase/PARP1 Apoptotic Signaling

To further validate whether HDAC8 genetically regulates apoptosis during VSMC calcification, we examined apoptosis after *Hdac8* knockdown. TUNEL staining showed that *Hdac8* knockdown decreased CM-induced TUNEL positivity, indicating that HDAC8 contributes to apoptosis under calcifying conditions (Figure 6A,B). Consistent with the TUNEL findings, Western blot analysis further demonstrated that Hdac8 knockdown significantly attenuated CM-induced PTEN protein upregulation and reduced the cleaved caspase-8/caspase-8 and cleaved caspase-3/caspase-3 ratios (Figure 6C–F). These findings provide additional genetic evidence linking HDAC8 expression to PTEN-associated caspase activation under calcifying conditions.

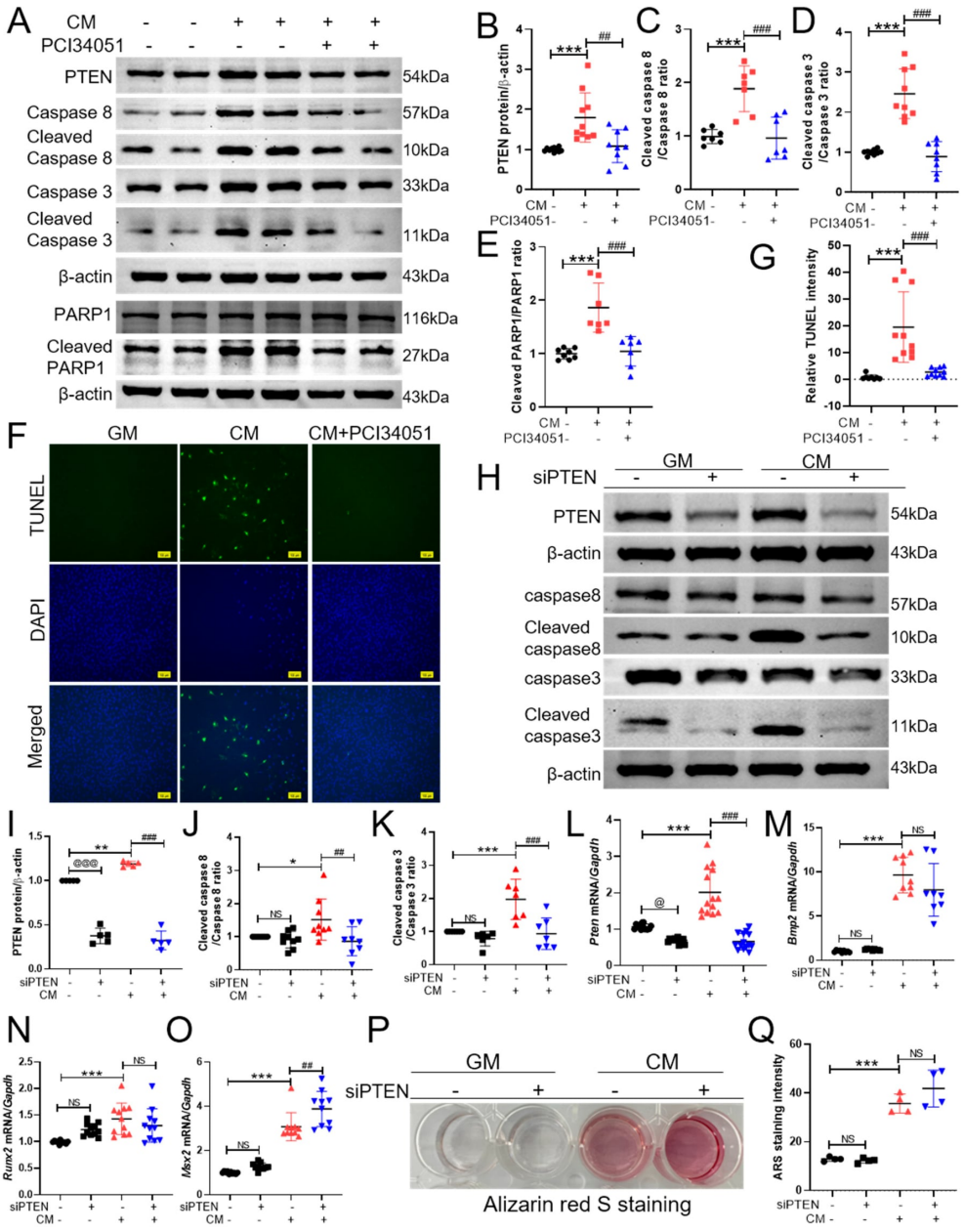


Figure 5. PTEN contributes to caspase-associated apoptotic signaling during VSMC calcification. (**A**–**E**) Representative Western blot images and densitometric analysis of PTEN, cleaved caspase-8/caspase-8, cleaved caspase-3/caspase-3, and cleaved PARP1/PARP1 in VSMCs cultured in GM or CM for 4 days followed by treatment with vehicle or PCI-34051 (0.1 μM) added during the final 24 h (n = 6–10). (**F**,**G**) Representative TUNEL staining and quantification in VSMCs cultured in GM or CM for 4 days, with vehicle or PCI-34051 (0.1 μM) added during the final 24 h (n = 8–10). Scale bar: 100 μm. (**H**–**K**) Representative Western blot images and densitometric analysis of PTEN, cleaved caspase-8/caspase-8, and cleaved caspase-3/caspase-3 in VSMCs transfected with siControl or siPTEN for 48 h and subsequently cultured in GM or CM for 4 days (n = 5–12). (**L**–**O**) qRT-PCR analysis of *Pten*, *Bmp2*, *Runx2*, and *Msx2* mRNA expression under the same conditions (n = 10–14). (**P**,**Q**) Representative Alizarin Red S staining images (**P**) and quantification of staining intensity (**Q**) in VSMCs transfected with siControl or siPTEN for 48 h and subsequently cultured in GM or CM for 4 days (n = 4). Staining intensity was calculated using ImageJ as the difference between the mean red- and green-channel intensities within a central circular region of interest in each well. Data are presented as mean ± SD. Each dot represents one independent biological experiment. $^{@}$ $p < 0.05$; $^{@@@}$ $p < 0.001$; * $p < 0.05$; ** $p < 0.01$; *** $p < 0.001$; $^{\#\#}$ $p < 0.01$; $^{\#\#\#}$ $p < 0.001$. GM, growth medium; CM, calcification medium.

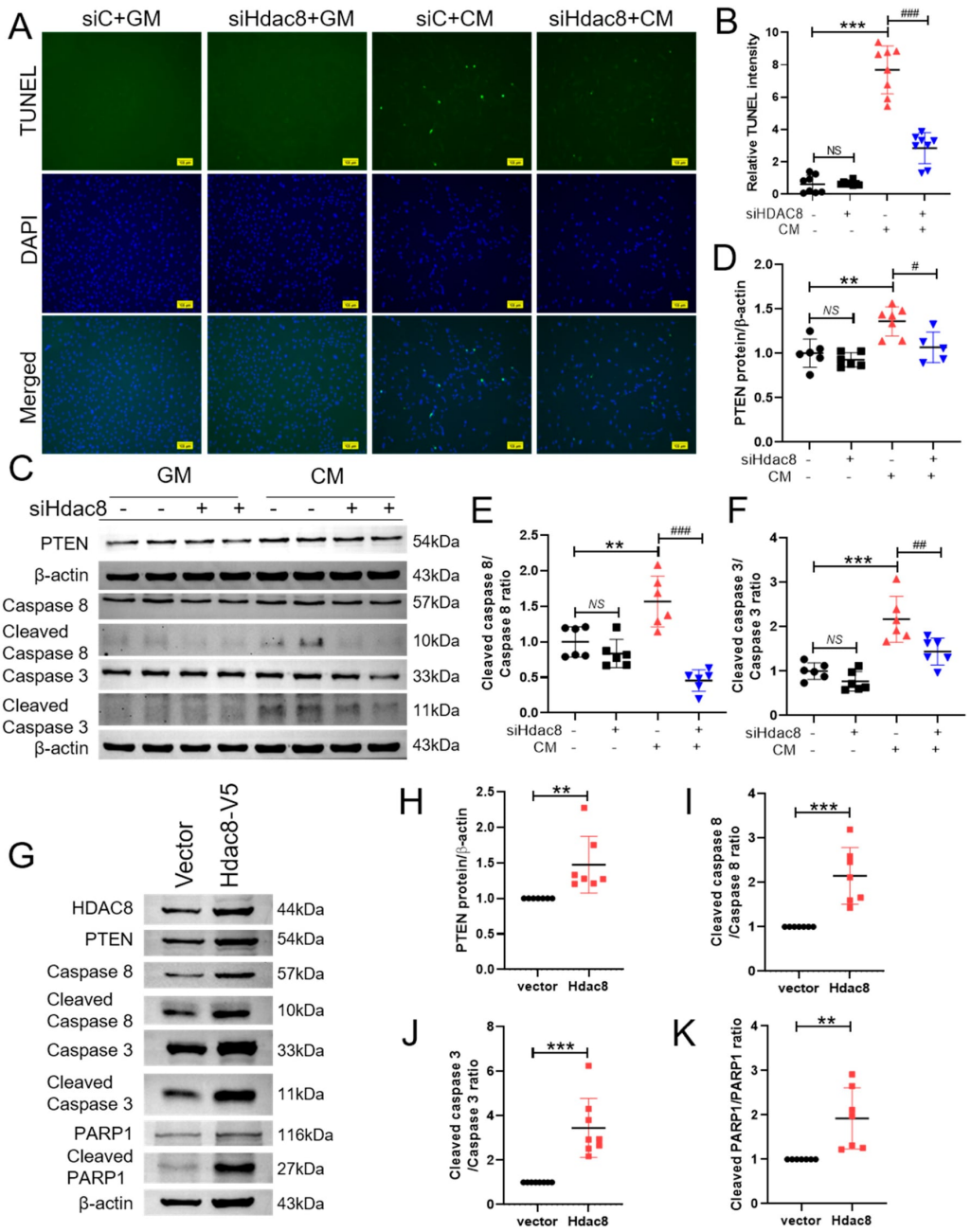


Figure 6. Genetic modulation of HDAC8 regulates PTEN expression and caspase-associated apoptotic signaling in VSMCs. (**A**,**B**) Representative TUNEL staining and quantification in VSMCs transfected with siControl or siHdac8 and cultured in GM or CM ($n = 8$). Scale bar: 100 μm. (**C**) Representative Western blot images of PTEN, caspase-8, cleaved caspase-8, caspase-3, and cleaved caspase-3 in VSMCs transfected with siControl or siHdac8 and subsequently exposed to GM or CM, with β-actin as the loading control. (**D**–**F**) Densitometric quantification of PTEN protein expression normalized to β-actin (**D**), cleaved caspase-8/caspase-8 ratio (**E**), and cleaved caspase-3/caspase-3 ratio (**F**) under the conditions described in (**C**) ($n = 5$–7). (**G**–**K**) Representative Western blot images of HDAC8, PTEN, caspase-8, cleaved caspase-8, caspase-3, cleaved caspase-3, PARP1, and cleaved PARP1, and densitometric analysis of PTEN and the corresponding cleaved/total protein ratios in A10 cells transfected with empty vector or an *Hdac8* expression plasmid for 48 h ($n = 5$–7). HDAC8 was included to confirm successful overexpression. Data are presented as mean ± SD. Each dot represents one independent biological experiment. ** $p < 0.01$; *** $p < 0.001$; $^{\#}$ $p < 0.05$; $^{\#\#}$ $p < 0.01$; $^{\#\#\#}$ $p < 0.001$. GM, growth medium; CM, calcification medium.

Conversely, in HDAC8-overexpressing A10 cells, PTEN protein abundance was increased, accompanied by enhanced caspase-dependent apoptotic signaling, as demonstrated by increased cleaved caspase-8/caspase-8, cleaved caspase-3/caspase-3, and cleaved PARP1/PARP1 ratios (Figure 6G–K). Together, these loss- and gain-of-function findings support the conclusion that HDAC8 promotes apoptotic signaling associated with PTEN upregulation and caspase/PARP1 cleavage in VSMCs.

3.7. PCI-34051 Attenuates Vitamin D_3-Induced Aortic Calcification and Osteogenic Marker Expression In Vivo

To determine whether PCI-34051 protects against vascular calcification in vivo, we used a vitamin D_3-induced mouse model of arterial calcification (Figure 7A). Vitamin D_3 administration markedly increased calcium deposition in the ascending aorta and aortic arch, as measured by quantification of aortic calcium content. PCI-34051 treatment significantly reduced vitamin D_3-induced aortic calcium accumulation (Figure 7B).

We next examined whether PCI-34051 attenuates osteogenic reprogramming in calcified aortic tissue. qRT-PCR analysis showed that vitamin D_3 increased the expression of *Runx2*, *Hdac8*, *Bmp2*, and *Msx2* in aortic tissue, whereas PCI-34051 significantly reduced these increases (Figure 7C–F). Consistent with the mRNA findings, vitamin D_3-treated mice exhibited increased protein expression of RUNX2, HDAC8, BMP2, and MSX2, as determined by Western blot analysis. PCI-34051 treatment significantly attenuated these increases (Figure 7G–K).

Histological analyses further confirmed the protective effect of PCI-34051. H&E staining showed that vitamin D_3 induced morphological alterations in the aortic media, whereas PCI-34051 partially preserved aortic medial morphology. Quantitative analysis further demonstrated that vitamin D_3 significantly reduced aortic wall thickness, whereas PCI-34051 treatment partially restored it (Figure 7L,M). Von Kossa staining demonstrated prominent medial calcification in vitamin D_3-treated mice, which was markedly reduced by PCI-34051 treatment, as confirmed by quantitative analysis of the Von Kossa-positive area (Figure 7N). Similarly, Alizarin Red S staining revealed increased medial calcium deposition following vitamin D_3 administration, which was significantly attenuated by PCI-34051 treatment (Figure 7O). These findings indicate that PCI-34051 reduces vitamin D_3-induced aortic calcium deposition, attenuates medial morphological alterations, and suppresses osteogenic reprogramming in vivo.

3.8. PCI-34051 Suppresses Both NOX2–AKT Activation and PTEN–Associated Caspase/PARP1 Apoptotic Signaling In Vivo

We next examined whether the two HDAC8-regulated signaling programs identified in vitro were also activated in vitamin D_3-induced vascular calcification in vivo. TUNEL staining showed that vitamin D_3 markedly increased apoptosis in the aortic media, whereas PCI-34051 significantly reduced vitamin D_3-induced TUNEL positivity (Figure 8A,B).

Western blot analysis demonstrated that vitamin D_3 increased NOX2 expression and enhanced AKT phosphorylation in aortic tissue. PCI-34051 attenuated vitamin D_3-induced NOX2 upregulation and reduced the increase in the p-AKT/AKT ratio (Figure 8C–E). We further examined ERK1 expression and phosphorylation in aortic tissues. Vitamin D_3 increased p-ERK1 and total ERK1 abundance, whereas PCI-34051 reduced both protein signals. However, the p-ERK1/ERK1 ratio was not decreased following PCI-34051 treatment and instead showed a relative increase (Supplementary Figure S2A–D). These findings suggest that HDAC8 inhibition suppresses NOX2-associated AKT activation in calcified aortas.

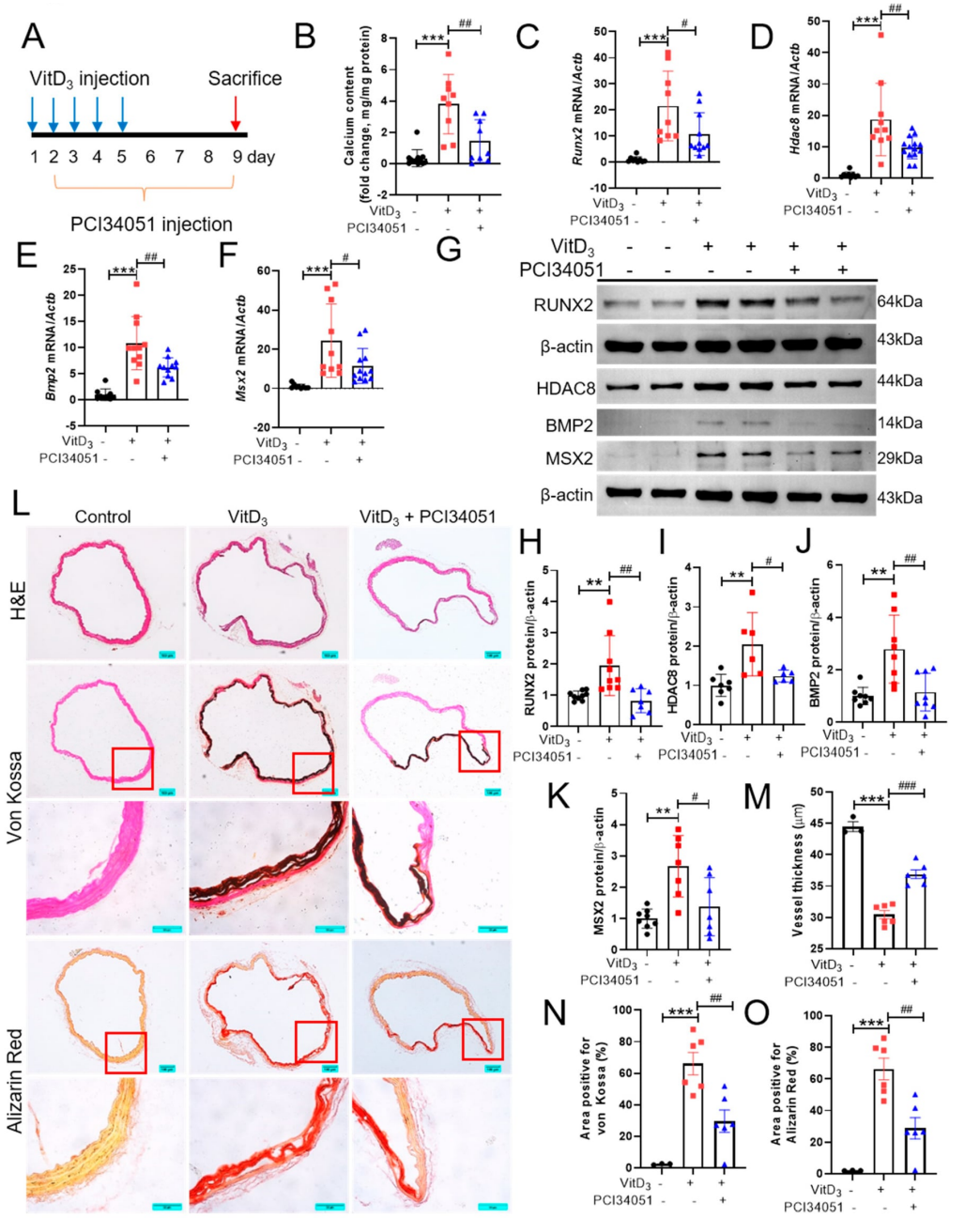


Figure 7. PCI-34051 attenuates vitamin D_3-induced aortic calcification and osteogenic marker expression in vivo. (**A**) Schematic of the vitamin D_3–induced calcification protocol and PCI-34051 treatment regimen. (**B**) Calcium content in the ascending aorta and aortic arch after decalcification in 0.6 N HCl for 24 h, measured using a colorimetric calcium assay (n = 9–12). (**C**–**F**) qRT-PCR analysis of *Runx2*, *Hdac8*, *Bmp2*, and *Msx2* mRNA expression in aortic tissue (n = 9–12). (**G**) Representative Western blot images of RUNX2, HDAC8, BMP2, and MSX2, with β-actin as the loading control. (**H**–**K**) Densitometric analysis of RUNX2, HDAC8, BMP2, and MSX2 protein levels normalized to β-actin (n = 6–8). (**L**) Representative images of hematoxylin and eosin (H&E) staining, von Kossa staining and Alizarin Red S staining of aortic sections from control, vitamin D_3-treated, and vitamin D_3 + PCI-34051-treated mice. For von Kossa and Alizarin Red S staining, the upper and lower panels show low- and high-magnification images, respectively. Scale bars: 100 μm (low magnification) and 50 μm (high magnification). (**M**) Quantification of medial thickness from H&E-stained sections (n = 3–6). (**N**) Quantification of von Kossa-positive calcified areas (n = 3–6). (**O**) Quantification of Alizarin Red S-positive calcified areas (n = 3–6). Data are presented as mean ± SD. ** $p < 0.01$; *** $p < 0.001$; $^{\#}$ $p < 0.05$; $^{\#\#}$ $p < 0.01$; $^{\#\#\#}$ $p < 0.001$. Each dot represents one individual aortic sample (not a technical replicate).

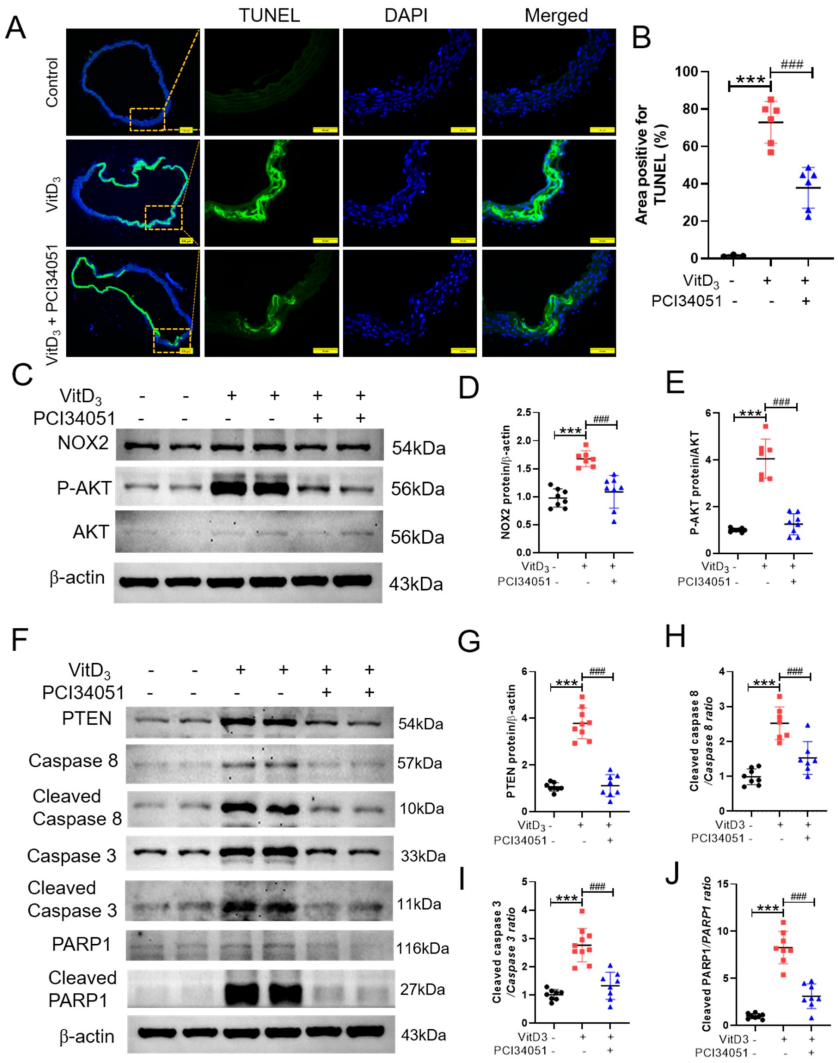


Figure 8. PCI-34051 suppresses both NOX2–AKT activation and PTEN-associated caspase/PARP1 apoptotic signaling in vivo. (**A**,**B**) Representative low-magnification overview images and corresponding higher-magnification (40×) fluorescence images of TUNEL staining (green), DAPI nuclear counterstaining (blue), and merged images in aortic sections from control, vitamin D_3-treated, and vitamin D_3 + PCI-34051-treated mice. Yellow dashed boxes indicate the regions selected for higher-magnification imaging. Quantification of TUNEL-positive areas is shown in (**B**) (n = 3–6). Scale bar: 100 µm, 50 µm. (**C**–**E**) Representative Western blot images and densitometric quantification of NOX2 and the p-AKT/AKT ratio in aortic tissues (n = 7–8). (**F**–**J**) Representative Western blot images and densitometric quantification of PTEN, cleaved caspase-8/caspase-8, cleaved caspase-3/caspase-3, and cleaved PARP1/PARP1 in the same aortic tissues (n = 8–9). The same protein samples were used for the Western blot analyses shown in Figure 8C,F, and identical β-actin bands were presented in both panels as a shared loading control. Data are presented as mean ± SD. Each dot represents one individual aortic sample. *** $p < 0.001$; ### $p < 0.001$.

In parallel, vitamin D_3 increased PTEN protein expression and enhanced caspase/PARP1 apoptotic signaling, as shown by increased cleaved caspase-8/caspase-8, cleaved caspase-3/caspase-3, and cleaved PARP1/PARP1 ratios. PCI-34051 significantly reduced these vitamin D_3-induced apoptotic signals (Figure 8F–J). Collectively, these findings indicate that the protective effect of PCI-34051 against vascular calcification in vivo is associated with suppression of both NOX2-associated AKT activation and PTEN-associated caspase/PARP1 apoptotic signaling.

3.9. Public Human VSMC Transcriptomic Analysis Reveals Oxidative Stress-Associated and Extracellular Matrix Remodeling Signatures During Osteogenic Differentiation

To assess the translational relevance of our experimental observations, we analyzed the public human VSMC osteogenic differentiation dataset GSE37558. In the day 12 versus day 0 comparison, volcano plot analysis revealed broad transcriptional remodeling. Genes associated with oxidative stress-related signaling, PTEN regulation, extracellular matrix remodeling, and VSMC phenotypic modulation, including *NOX4, PTEN*, *COL8A1, LUM*, and *PDGFD*, were highlighted (Figure 9A). Notably, *NOX4* was significantly upregulated in the day 12 versus day 0 comparison, whereas *CYBB* (encoding *NOX2*) did not exhibit significant differential expression.

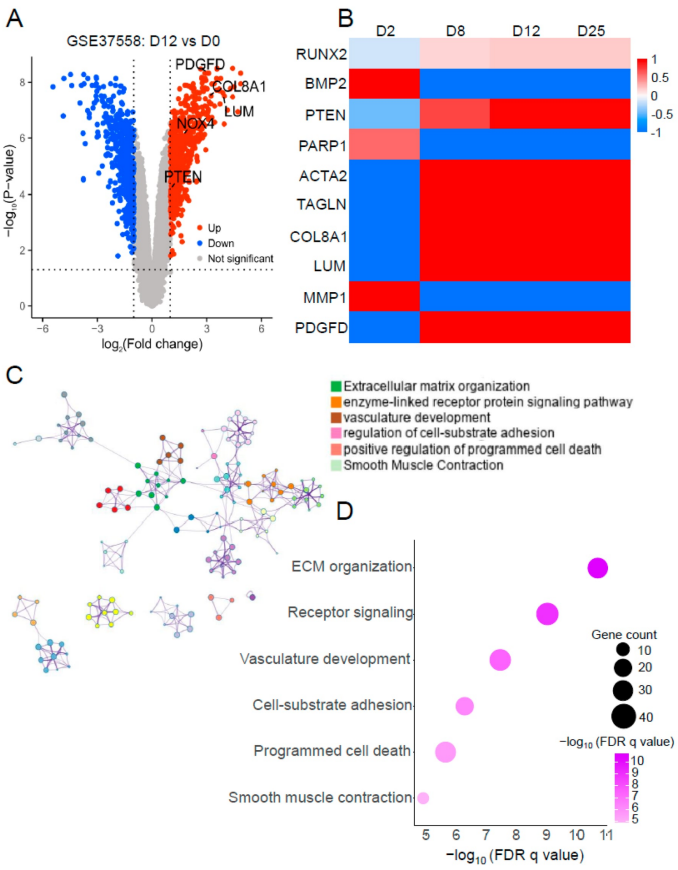


Figure 9. Public human VSMC transcriptomic analysis reveals oxidative stress-associated and extracellular matrix remodeling signatures during osteogenic differentiation. (**A**) Volcano plot of differentially expressed genes in GSE37558 at day 12 versus day 0. Upregulated genes are shown in red, downregulated genes in blue, and non-significant genes in gray. Significance was defined as an adjusted p value < 0.05 and an absolute log2 fold change ≥ 1. Selected genes associated with oxidative stress, apoptosis-related signaling, extracellular matrix remodeling, and VSMC pathological remodeling, including *NOX4, PTEN, COL8A1, LUM*, and *PDGFD*, are labeled. (**B**) Time-course heatmap showing original $\log_2$ fold-change values of selected genes relative to day 0. No row-wise scaling was applied. Red indicates upregulation, blue indicates downregulation, and white indicates little or no change. D2, D8, D12, and D25 represent day 2, day 8, day 12, and day 25 of osteogenic induction, respectively. (**C**) Enrichment network of significantly upregulated genes from the day 12 versus day 0 comparison. Nodes represent enriched terms or pathways, and connected nodes indicate functional similarity based on shared gene membership. (**D**) Bubble plot summarizing representative enriched GO Biological Process and Reactome terms. The x-axis represents −log10(FDR q value), bubble size indicates the number of upregulated genes mapped to each term, and color intensity reflects enrichment significance.

Time-course heatmap analysis showed stage-dependent transcriptional remodeling during human VSMC osteogenic differentiation. Extracellular matrix and VSMC remodeling-associated genes, including *RUNX2, ACTA2, TAGLN, COL8A1, LUM*, and *PDGFD*, showed relatively higher expression at later time points, whereas PTEN also exhibited higher expression at later stages. In contrast, *BMP2, PARP1,* and *MMP1* displayed distinct temporal regulation. These patterns suggest coordinated extracellular matrix remodeling, VSMC phenotypic modulation, and *PTEN*-associated transcriptional changes during human VSMC osteogenic differentiation (Figure 9B).

Functional enrichment analysis of significantly upregulated genes in the day 12 versus day 0 comparison identified major biological clusters related to extracellular matrix organization, enzyme-linked receptor protein signaling, vasculature development, cell–substrate adhesion, positive regulation of programmed cell death, and smooth muscle contraction (Figure 9C). These enriched themes were further summarized by bubble plot analysis (Figure 9D). Together, these transcriptomic findings identify gene expression patterns associated with oxidative stress-related signaling, extracellular matrix remodeling, VSMC phenotypic modulation, and cell fate regulation during human VSMC osteogenic differentiation, providing supportive transcriptomic context for our experimental findings.

4. Discussion

Vascular calcification is increasingly recognized as an active, cell-regulated process rather than a passive degenerative event, with medial vascular smooth muscle cells (VSMCs) serving as key effectors of osteogenic reprogramming, matrix mineralization, apoptosis, and arterial wall stiffening [1,5–8]. In the present study, we demonstrate that HDAC8 contributes to medial vascular calcification in association with oxidative stress-related and apoptotic signaling responses. In calcifying VSMCs and in a vitamin D_3-induced mouse model of arterial medial calcification, HDAC8-associated changes involved two complementary signaling responses: NOX2/ROS–AKT signaling associated with osteogenic remodeling and PTEN-associated caspase/PARP1 apoptotic signaling associated with VSMC injury. Isoform-selective HDAC8 inhibition with PCI-34051 attenuated mineral deposition, osteogenic marker induction, ROS accumulation, and apoptosis in calcifying VSMCs, as well as aortic calcification, osteogenic remodeling, and apoptotic injury in vivo, while Hdac8 knockdown further supported the involvement of HDAC8 in VSMC calcification, oxidative stress, and apoptosis.

An important finding of this study is that HDAC8 appears to be associated with multiple signaling responses during vascular calcification rather than a single linear downstream pathway. Although PTEN is classically recognized as a negative regulator of PI3K–AKT signaling, our findings are not readily explained by a simple model in which HDAC8 activates PTEN to suppress AKT. Instead, calcifying stress increased AKT phosphorylation, PTEN expression, and caspase/PARP1 cleavage, all of which were attenuated by HDAC8 inhibition. These observations suggest that HDAC8 is involved in two concurrent signaling responses: NOX2/ROS-associated AKT activation, which may contribute to osteogenic remodeling under calcifying conditions, and PTEN-associated caspase/PARP1 signaling, which is linked to apoptotic injury. Although AKT is generally recognized as a pro-survival kinase, its downstream effectors may mediate distinct cellular responses. In a calcium/phosphate-induced VSMC calcification model, increased AKT phosphorylation was associated with enhanced FOXO3a phosphorylation and degradation, reduced apoptosis, and attenuated calcification [39]. In our model, increased AKT phosphorylation may reflect a compensatory survival response and/or signaling associated with osteogenic remodeling without necessarily preventing apoptosis. However, the functional contribution of AKT activation and the involvement of FOXO3a remain to be established. Furthermore, increased PTEN protein

abundance does not necessarily indicate enhanced PTEN phosphatase activity, which is subject to redox and post-translational regulation [40]. Together, these findings suggest that NOX2/ROS-associated AKT activation and PTEN-associated apoptotic signaling may represent distinct but potentially interconnected responses to calcifying stress, rather than components of an established linear signaling pathway. However, direct causal interactions between these signaling responses have not been demonstrated, and further targeted genetic and rescue experiments are required to clarify their functional relationships.

These findings add HDAC8 to the broader, isoform-specific landscape of HDAC regulation in vascular calcification. Prior studies have demonstrated context-dependent roles for multiple HDACs, including HDAC2 as potentially protective in CKD-associated calcification via autophagy [41], HDAC1 degradation facilitating osteogenic conversion [42], focal adhesion signaling linked to HDAC4/5 [43], and HDAC5 involvement in microRNA-dependent mineralization [44]. Beyond medial calcification, HDAC6 has also been implicated in valvular and endothelial stress phenotypes [45,46], whereas HDAC9 appears to exert divergent roles depending on the calcification context, including medial calcification and CKD-associated settings [47,48]. Together, these observations underscore the complexity of HDAC isoform-specific functions and suggest that selective targeting of individual HDACs may offer advantages over nonselective inhibition in calcification-prone vascular disease. In this context, PCI-34051 serves as a useful pharmacological tool for investigating HDAC8-associated mechanisms and provides a rationale for further evaluating selective HDAC8 inhibition as a potential therapeutic approach to vascular calcification.

HDAC8 may reflect distinct mechanisms of intervention. Recent studies have highlighted deacetylase-independent functions of HDAC8, suggesting that inhibition of its catalytic activity may not fully reproduce the effects of protein depletion [49]. Furthermore, HDAC1/2 have been implicated in the epigenetic repression of RUNX2 transcription through promoter-associated regulatory complexes [50]. Although the increased Hdac1 expression following Hdac8 knockdown may indicate a compensatory transcriptional response, its functional contribution remains uncertain. Additional cellular effects of PCI-34051, as reported in recent pharmacological studies, may also contribute to the discrepancy [51]. Further investigation is needed to distinguish these potential mechanisms.

Mechanistically, our data support a NOX2-associated redox signaling response linked to HDAC8. Oxidative stress and NADPH oxidases are established drivers of VSMC osteogenic switching [10–12], and AKT signaling has been linked to ROS-associated osteogenic remodeling and RUNX2-related calcification programs [14]. Accordingly, AKT was investigated primarily because of its established involvement in ROS-associated osteogenic reprogramming and vascular calcification, rather than solely as a regulator of cell survival or proliferation. In our model, calcifying conditions increased ROS accumulation, *Nox2* mRNA expression, NOX2 protein abundance, and AKT phosphorylation. PCI-34051 reduced NOX2 expression and AKT phosphorylation, while *Hdac8* knockdown decreased *Nox2* mRNA expression and *Hdac8* overexpression increased NOX2 protein abundance and AKT phosphorylation. In addition, the NOX2 inhibitor GSK2795039 reduced CM-induced DHE fluorescence, supporting the involvement of NOX2 activity in calcification-associated ROS accumulation. Although our in vitro antioxidant and NOX2 inhibitor experiments support the involvement of ROS in calcification-associated responses, the effects of antioxidant intervention on AKT phosphorylation and vascular calcification were not evaluated in vivo. Further studies combining antioxidant treatment or targeted NOX2 inhibition with the vitamin D_3-induced calcification model are needed to clarify the functional contribution of NOX2/ROS signaling to AKT activation and vascular calcification. Although calcifying cues may affect multiple NOX isoforms, the changes associated with HDAC8 modulation in our experimental system were most consistently observed in NOX2 expression, ROS

accumulation, and AKT phosphorylation. The regulation of NOX isoforms appears to be context-dependent rather than strictly selective for NOX2, consistent with previous evidence implicating other NOX isoforms in VSMC phenotypic switching and vascular calcification [52]. The distinct NOX expression patterns observed between our experimental models and the human GSE37558 dataset may reflect differences in the duration of osteogenic induction, experimental conditions, and isoform-specific regulatory mechanisms. Importantly, GSE37558 reflects osteogenic differentiation without HDAC8 manipulation and therefore provides evidence of broader oxidative stress-associated transcriptional remodeling rather than direct validation of HDAC8–NOX2 signaling.

Alongside the NOX2/ROS–AKT-associated response, HDAC8 was also implicated in PTEN-associated caspase/PARP1 apoptotic signaling. Apoptotic VSMC injury is recognized as an important contributor to medial calcification because apoptotic bodies and membrane fragments can provide nucleation sites for calcium phosphate deposition [5–8]. In our study, CM and vitamin D_3 increased PTEN expression and caspase-8, caspase-3, and PARP1 cleavage. PCI-34051 reduced these apoptotic signals both in vitro and in vivo, while Hdac8 knockdown attenuated CM-induced TUNEL positivity, PTEN protein upregulation, and caspase-8 and caspase-3 cleavage, further supporting the involvement of HDAC8 in apoptosis-associated signaling. Importantly, PTEN knockdown attenuated caspase-8 and caspase-3 cleavage under calcifying conditions but did not suppress CM-induced *Bmp2* or *Runx2* mRNA expression. These findings suggest that PTEN-associated caspase activation and osteogenic mineralization may be differentially regulated, as attenuation of caspase activation following Pten knockdown was not accompanied by an apparent reduction in osteogenic marker expression or mineral deposition. Although the relationship between oxidative/AKT signaling and PTEN-associated apoptosis remains unresolved, these findings suggest that PTEN-associated apoptotic signaling and osteogenic marker induction may be differentially regulated during VSMC calcification. Consistent with the established involvement of caspase activation in apoptosis, the observed cleavage of caspase-8, caspase-3, and PARP1 further supports a role for caspase-associated signaling in calcification-related VSMC injury [53].

The in vivo findings strengthen the pathophysiological relevance of HDAC8-associated oxidative and apoptotic signaling in medial vascular calcification. In vitamin D_3-treated mice, PCI-34051 attenuated aortic calcium accumulation, osteogenic marker expression, and medial calcification, as demonstrated by von Kossa and Alizarin Red S staining, while partially preserving medial architecture. These structural improvements were accompanied by reduced NOX2 expression and AKT phosphorylation, attenuation of PTEN-associated caspase/PARP1 apoptotic signaling, and a reduction in TUNEL-positive area in aortic tissue. Thus, the changes in oxidative stress-associated and apoptotic signaling observed in calcifying VSMCs were also reflected in the in vivo model, supporting the potential of HDAC8 inhibition to attenuate both osteogenic remodeling and apoptosis-associated medial injury.

Public transcriptomic analysis of GSE37558 provided an independent human VSMC context for interpreting our experimental findings. Rather than indicating a simple osteogenic switch alone, the human osteogenic differentiation profile suggested a broader transcriptional response involving extracellular matrix reorganization, VSMC phenotypic modulation, changes in PTEN expression, and programmed cell death-associated biological processes. The increased expression of contractile markers during later stages of osteogenic differentiation suggests that VSMC phenotypic switching may not necessarily involve a complete loss of smooth muscle identity. Previous studies have demonstrated that VSMCs can retain contractile characteristics alongside osteogenic-associated remodeling [54,55]. These findings highlight the dynamic and context-dependent nature of VSMC

phenotypic plasticity, although bulk transcriptomic data cannot resolve whether these molecular programs coexist within individual cells. This pattern is broadly consistent with our experimental data showing that HDAC8-associated changes involve ROS accumulation, osteogenic remodeling, apoptosis-associated signaling, and medial structural disruption during vascular calcification. Importantly, the observed changes in PTEN expression and enrichment of programmed cell death-associated processes suggest that apoptosis-related transcriptional responses may accompany osteogenic reprogramming during calcification. Because GSE37558 was not designed to test HDAC8 inhibition or PCI-34051 treatment, these transcriptomic data should be interpreted as supportive rather than causal. Nevertheless, evidence of broader cellular remodeling processes consistent with, but not directly validating, the signaling changes observed in our experimental models.

From a translational perspective, our results suggest that isoform-selective HDAC8 inhibition may represent a potential strategy to mitigate both calcification-associated remodeling and medial injury. Given the diverse and sometimes opposing roles of HDAC isoforms in vascular cells, selective HDAC8 targeting may offer a more focused therapeutic approach than broad HDAC inhibition, although its comparative safety and efficacy remain to be established [19–24,41–43,45,47,48]. These findings support the potential therapeutic relevance of HDAC8 inhibition in vascular calcification. However, the in vitro VSMC model and the high-dose vitamin D_3-induced mouse model do not fully recapitulate the chronic and multifactorial nature of human vascular calcification. In addition, PCI-34051 was administered for only 7 days, and its long-term tolerability and potential effects on vital organ functions were not systematically evaluated. Given the reported pharmacokinetic limitations of PCI-34051 [56], prolonged treatment studies assessing systemic toxicity, organ function, and therapeutic efficacy in chronic vascular calcification models are warranted before clinical translation.

Several limitations should be considered. Although PCI-34051 is widely used as a selective HDAC8 inhibitor and our genetic gain- and loss-of-function experiments support the involvement of HDAC8, VSMC-specific *Hdac8* deletion in vivo would provide more definitive evidence. Furthermore, serum calcium, phosphate, PTH, and calcitonin levels were not assessed in the vitamin D_3-induced calcification model. Therefore, potential contributions of systemic alterations in mineral metabolism to the observed vascular calcification and the protective effects of PCI-34051 cannot be excluded. In addition, the necessity of NOX2 and the precise crosstalk between the NOX2/ROS–AKT and PTEN–caspase programs require further validation using targeted rescue or genetic approaches. Although additional analyses revealed changes in ERK1 protein abundance and phosphorylation, PCI-34051 did not reduce the p-ERK1/ERK1 ratio. Moreover, VSMC proliferation was not directly assessed in vivo, and therefore the potential involvement of ERK1-dependent proliferative responses in the effects of HDAC8 inhibition remains unresolved. Finally, the public human VSMC transcriptomic analysis provides supportive context rather than direct validation of PCI-34051 or HDAC8-dependent mechanisms in human medial calcification.

In conclusion, our findings support a role for HDAC8 in medial vascular calcification, associated with NOX2/ROS–AKT-related oxidative and osteogenic remodeling and PTEN-associated caspase/PARP1 apoptotic signaling. Isoform-selective HDAC8 inhibition with PCI-34051 attenuates these signaling responses, reduces VSMC calcification and vitamin D_3-induced aortic calcification, and partially preserves aortic medial architecture. These findings support HDAC8 as a potential therapeutic target for oxidative stress-associated medial vascular calcification.

Supplementary Materials: The following supporting information can be downloaded at https://www.mdpi.com/article/10.3390/antiox15121568/s1. Supplementary Table S1: Full differential expression results for GSE37558 (D12 versus D0); Supplementary Table S2: Curated mechanism-

related gene panel and original log2 fold-change values used for the time-course heatmap in GSE37558; Supplementary Table S3: Representative enriched terms and pathways of upregulated genes in GSE37558 (D12 versus D0); Supplementary Figure S1. Effects of Hdac8 knockdown on the expression of other class I HDACs in vascular smooth muscle cells. Supplementary Figure S2. Effects of PCI-34051 on ERK1 expression and phosphorylation in vitamin D_3-induced vascular calcification.

Author Contributions: H.Z.: Conceptualization, Methodology, Investigation, Writing—original draft. H.J.K.: Conceptualization, Supervision, Funding acquisition, Visualization, Writing—review and editing. L.W.: Investigation. S.H.L.: Writing—review and editing. S.H.K.: Investigation. M.H.J.: Writing—review and editing. Y.J.H.: Writing—review and editing, Supervision, Funding acquisition. All authors have read and agreed to the published version of the manuscript.

Funding: This work was supported by the National Research Foundation of Korea (NRF) grant funded by the Korean government (RS-2022-NR069133); the Korea Health Technology R&D Project through the Korea Health Industry Development Institute (KHIDI), funded by the Ministry of Health and Welfare, Republic of Korea (RS-2025-24536036); and an additional grant from the Ministry of Health and Welfare, Republic of Korea (RS-2023-00302153).

Institutional Review Board Statement: All animal experiments were approved by the Institutional Animal Care and Use Committee of Chonnam National University Medical School (CNUH IACUC-22023, approved on 26 September 2022). All procedures were performed in accordance with the National Institutes of Health Guide for the Care and Use of Laboratory Animals (8th edition, 2011) and complied with institutional and national regulations governing the ethical use of animals in research.

Data Availability Statement: The original contributions presented in this study are included in the article and Supplementary Material. The publicly available transcriptomic dataset analyzed in this study can be accessed through the Gene Expression Omnibus (GEO) under accession number GSE37558. Further inquiries can be directed to the corresponding author.

Acknowledgments: During the preparation of this manuscript, the authors used ChatGPT-6. (OpenAI. San Francisco, CA, USA) to improve the clarity and grammar of the English text. After using this tool, the authors carefully reviewed and edited the content, and the authors take full responsibility for the final version of the manuscript.

Conflicts of Interest: The authors declare a familial relationship between two co-authors: Hae Jin Kee is the mother of Seong Hoon Kim. This relationship did not influence the study design, data collection, analysis, interpretation, or manuscript preparation. All scientific procedures were performed independently, and the integrity and objectivity of the work were maintained throughout the study. The authors declare no financial conflicts of interest.

References

1. Lee, S.J.; Lee, I.K.; Jeon, J.H. Vascular Calcification—New Insights Into Its Mechanism. *Int. J. Mol. Sci.* **2020**, *21*, 2685. [CrossRef] [PubMed]
2. Muyor, K.; Laget, J.; Cortijo, I.; Duranton, F.; Jover, B.; Argilés, À.; Gayrard, N. Vascular calcification in different arterial beds in ex vivo ring culture and in vivo rat model. *Sci. Rep.* **2022**, *12*, 11861. [CrossRef] [PubMed]
3. Cheng, H.M.; Wang, J.J.; Chen, C.H. The Role of Vascular Calcification in Heart Failure and Cognitive Decline. *Pulse* **2018**, *5*, 144–153. [CrossRef] [PubMed]
4. Leening, M.J.; Elias-Smale, S.E.; Kavousi, M.; Felix, J.F.; Deckers, J.W.; Vliegenthart, R.; Oudkerk, M.; Hofman, A.; Steyerberg, E.W.; Stricker, B.H.; et al. Coronary calcification and the risk of heart failure in the elderly: The Rotterdam Study. *JACC Cardiovasc. Imaging* **2012**, *5*, 874–880. [CrossRef] [PubMed]
5. Demer, L.L.; Tintut, Y. Vascular calcification: Pathobiology of a multifaceted disease. *Circulation* **2008**, *117*, 2938–2948. [CrossRef] [PubMed]
6. Lanzer, P.; Hannan, F.M.; Lanzer, J.D.; Janzen, J.; Raggi, P.; Furniss, D.; Schuchardt, M.; Thakker, R.; Fok, P.W.; Saez-Rodriguez, J.; et al. Medial Arterial Calcification: JACC State-of-the-Art Review. *J. Am. Coll. Cardiol.* **2021**, *78*, 1145–1165. [CrossRef] [PubMed]
7. Lanzer, P.; Boehm, M.; Sorribas, V.; Thiriet, M.; Janzen, J.; Zeller, T.; St Hilaire, C.; Shanahan, C. Medial vascular calcification revisited: Review and perspectives. *Eur. Heart J.* **2014**, *35*, 1515–1525. [CrossRef] [PubMed]
8. Qian, Y.; Li, L.; Sun, Z.; Liu, J.; Yuan, W.; Wang, Z. A multi-omics view of the complex mechanism of vascular calcification. *Biomed. Pharmacother.* **2021**, *135*, 111192. [CrossRef] [PubMed]

9. Xie, Y.; Lin, T.; Jin, Y.; Berezowitz, A.G.; Wang, X.L.; Lu, J.; Cai, Y.; Guzman, R.J. Smooth muscle cell-specific matrix metalloproteinase 3 deletion reduces osteogenic transformation and medial artery calcification. *Cardiovasc. Res.* **2024**, *120*, 658–670. [CrossRef] [PubMed]
10. Toth, A.; Balogh, E.; Jeney, V. Regulation of Vascular Calcification by Reactive Oxygen Species. *Antioxidants* **2020**, *9*, 963. [CrossRef] [PubMed]
11. Qiao, Y. Reactive Oxygen Species in Cardiovascular Calcification: Role of Medicinal Plants. *Front. Pharmacol.* **2022**, *13*, 858160. [CrossRef] [PubMed]
12. Lin, Y.; Zhang, H.; Jiang, Y.; Tian, W. Oxidative stress and its related epigenetic modifications in vascular calcification: Mechanisms and advances. *Front. Cardiovasc. Med.* **2025**, *12*, 1662989. [CrossRef] [PubMed]
13. Towler, D.A. Vascular calcification: It's all the RAGE! *Arterioscler. Thromb. Vasc. Biol.* **2011**, *31*, 237–239. [CrossRef] [PubMed]
14. Byon, C.H.; Javed, A.; Dai, Q.; Kappes, J.C.; Clemens, T.L.; Darley-Usmar, V.M.; McDonald, J.M.; Chen, Y. Oxidative Stress Induces Vascular Calcification through Modulation of the Osteogenic Transcription Factor Runx2 by AKT Signaling. *J. Biol. Chem.* **2008**, *283*, 15319–15327. [CrossRef] [PubMed]
15. Xu, W.; Wu, Y.; Mao, R.; Jia, Y.; Jiang, H.; Zhang, F.; Huang, D.; He, X.; Wang, C.; Huang, K. Poly(ADP-ribose) polymerase 1 orchestrates vascular smooth muscle cell homeostasis in arterial disease. *Exp. Mol. Med.* **2025**, *57*, 1686–1699. [CrossRef] [PubMed]
16. Zhu, Y.; Zhang, J.L.; Yan, X.J.; Ji, Y.; Wang, F.F. Exploring a new mechanism between lactate and VSMC calcification: PARP1/POLG/UCP2 signaling pathway and imbalance of mitochondrial homeostasis. *Cell Death Dis.* **2023**, *14*, 598. [CrossRef] [PubMed]
17. Zhang, F.; Xie, R.; Munoz, F.M.; Lau, S.S.; Monks, T.J. PARP-1 hyperactivation and reciprocal elevations in intracellular Ca^{2+} during ROS-induced nonapoptotic cell death. *Toxicol. Sci.* **2014**, *140*, 118–134. [CrossRef] [PubMed]
18. Liu, H.; Wang, L.; Pan, Y.; Wang, X.; Ding, Y.; Zhou, C.; Shah, A.M.; Zhao, G.; Zhang, M. Celastrol Alleviates Aortic Valve Calcification Via Inhibition of NADPH Oxidase 2 in Valvular Interstitial Cells. *JACC Basic Transl. Sci.* **2020**, *5*, 35–49. [CrossRef] [PubMed]
19. Yang, H.; Guo, K.; Ding, P.; Ning, J.; Zhang, Y.; Wang, Y.; Wang, Z.; Liu, G.; Shao, C.; Pan, M.; et al. Histone deacetylases: Regulation of vascular homeostasis via endothelial cells and vascular smooth muscle cells and the role in vascular pathogenesis. *Genes Dis.* **2024**, *11*, 101216. [CrossRef] [PubMed]
20. Zhao, T.C.; Wang, Z.; Zhao, T.Y. The important role of histone deacetylases in modulating vascular physiology and arteriosclerosis. *Atherosclerosis* **2020**, *303*, 36–42. [CrossRef] [PubMed]
21. Yan, H.; Yin, Y.; Zhou, Y.; Li, Z.; Li, Y.; Ren, L.; Wen, J.; Wang, W. Regulation of cardiovascular diseases by histone deacetylases and NADPH oxidases. *Redox Biol.* **2024**, *77*, 103379. [CrossRef] [PubMed]
22. Luan, Y.; Liu, H.; Luan, Y.; Yang, Y.; Yang, J.; Ren, K.D. New Insight in HDACs: Potential Therapeutic Targets for the Treatment of Atherosclerosis. *Front. Pharmacol.* **2022**, *13*, 863677. [CrossRef] [PubMed]
23. Feltran, G.D.S.; Alves Dos Santos, E.A.; de Camargo Andrade, A.F.; Zambuzzi, W.F.; da Silva, R.A.F. Epigenetic modulation of vascular calcification: Looking for comprehending the role of sirt1 and histone acetylation in VSMC phenotypic transition. *Exp. Cell Res.* **2024**, *443*, 114311. [CrossRef] [PubMed]
24. Kwon, D.H.; Ryu, J.; Kim, Y.K.; Kook, H. Roles of Histone Acetylation Modifiers and Other Epigenetic Regulators in Vascular Calcification. *Int. J. Mol. Sci.* **2020**, *21*, 3246. [CrossRef] [PubMed]
25. Findeisen, H.M.; Gizard, F.; Zhao, Y.; Qing, H.; Heywood, E.B.; Jones, K.L.; Cohn, D.; Bruemmer, D. Epigenetic regulation of vascular smooth muscle cell proliferation and neointima formation by histone deacetylase inhibition. *Arterioscler. Thromb. Vasc. Biol.* **2011**, *31*, 851–860. [CrossRef] [PubMed]
26. Zhao, T.; Kee, H.J.; Kee, S.J.; Jeong, M.H. Hdac8 Inhibitor Alleviates Transverse Aortic Constriction-Induced Heart Failure in Mice by Downregulating Ace1. *Oxidative Med. Cell. Longev.* **2022**, *2022*, 6227330. [CrossRef] [PubMed]
27. Kee, H.J.; Ryu, Y.; Seok, Y.M.; Choi, S.Y.; Sun, S.; Kim, G.R.; Jeong, M.H. Selective inhibition of histone deacetylase 8 improves vascular hypertrophy, relaxation, and inflammation in angiotensin II hypertensive mice. *Clin. Hypertens.* **2019**, *25*, 13. [CrossRef] [PubMed]
28. Papa, A.; Pandolfi, P.P. The PTEN-PI3K Axis in Cancer. *Biomolecules* **2019**, *9*, 153. [CrossRef] [PubMed]
29. Matsuda, S.; Nakanishi, A.; Wada, Y.; Kitagishi, Y. Roles of PI3K/AKT/PTEN Pathway as a Target for Pharmaceutical Therapy. *Open Med. Chem. J.* **2013**, *7*, 23–29. [CrossRef] [PubMed]
30. Alimohammadi, M.; Rahimzadeh, P.; Khorrami, R.; Bonyadi, M.; Daneshi, S.; Nabavi, N.; Raesi, R.; Farani, M.R.; Dehkhoda, F.; Taheriazam, A.; et al. A comprehensive review of the PTEN/PI3K/Akt axis in multiple myeloma: From molecular interactions to potential therapeutic targets. *Pathol. Res. Pract.* **2024**, *260*, 155401. [CrossRef] [PubMed]
31. Qi, Y.; Liu, J.; Saadat, S.; Tian, X.; Han, Y.; Fong, G.H.; Pandolfi, P.P.; Lee, L.Y.; Li, S. PTEN induces apoptosis and cavitation via HIF-2-dependent Bnip3 upregulation during epithelial lumen formation. *Cell Death Differ.* **2015**, *22*, 875–884. [CrossRef] [PubMed]

32. Ma, S.C.; Zhang, H.P.; Jiao, Y.; Wang, Y.H.; Zhang, H.; Yang, X.L.; Yang, A.N.; Jiang, Y.D. Homocysteine-induced proliferation of vascular smooth muscle cells occurs via PTEN hypermethylation and is mitigated by Resveratrol. *Mol. Med. Rep.* **2018**, *17*, 5312–5319. [CrossRef] [PubMed]
33. Li, M.; Wang, Z.W.; Fang, L.J.; Cheng, S.Q.; Wang, X.; Liu, N.F. Programmed cell death in atherosclerosis and vascular calcification. *Cell Death Dis.* **2022**, *13*, 467. [CrossRef] [PubMed]
34. Qi, R.Q.; Chen, Y.F.; Cheng, J.; Song, J.W.; Chen, Y.H.; Wang, S.Y.; Liu, Y.; Yan, K.X.; Liu, X.Y.; Li, J.; et al. Elabela alleviates cuproptosis and vascular calcification in vitaminD3- overloaded mice via regulation of the PPAR-γ/FDX1 signaling. *Mol. Med.* **2024**, *30*, 223. [CrossRef] [PubMed]
35. Li, C.; Yang, P.; Liu, X.; Chen, X.; Mei, S.; Yang, L.; Yin, G.; Li, S.; Tao, J.; Li, L.; et al. PDZ domain containing protein 1 aggravates mouse vascular smooth muscle cells calcification via PDZ1 domain mediated beta-catenin stabilization and nuclear translocation. *Commun. Biol.* **2025**, *8*, 1642. [CrossRef] [PubMed]
36. Kwon, D.H.; Choe, N.; Shin, S.; Ryu, J.; Kim, N.; Eom, G.H.; Nam, K.I.; Kim, H.S.; Ahn, Y.; Kim, Y.K.; et al. Regulation of MDM2 E3 ligase-dependent vascular calcification by MSX1/2. *Exp. Mol. Med.* **2021**, *53*, 1781–1791. [CrossRef] [PubMed]
37. Zhou, H.; Kee, H.J.; Jeong, S.M.; Bai, L.; Wan, L.; Kim, S.H.; Lee, S.H.; Kurz, T.; Sim, D.S.; Jeong, M.H.; et al. YAK577 Attenuates Vascular Calcification by Targeting an MMP14-NOX2/ROS Axis in VSMCs and a Vitamin D(3)-Induced Mouse Model. *Antioxidants* **2026**, *15*, 605. [CrossRef] [PubMed]
38. Chen, T.; Liu, Y.X.; Chen, T.; Yang, M.; Fan, S.; Shi, M.; Wei, B.; Lv, H.; Cao, W.; Wang, C.; et al. ImageGP 2 for enhanced data visualization and reproducible analysis in biomedical research. *iMeta* **2024**, *3*, e239. [CrossRef] [PubMed]
39. Li, Y.; Sun, W.; Saaoud, F.; Wang, Y.; Wang, Q.; Hodge, J.; Hui, Y.; Yin, S.; Lessner, S.M.; Kong, X.; et al. MiR155 modulates vascular calcification by regulating Akt-FOXO3a signalling and apoptosis in vascular smooth muscle cells. *J. Cell. Mol. Med.* **2021**, *25*, 535–548. [CrossRef] [PubMed]
40. Trinh, V.H.; Choi, J.M.; Nguyen Huu, T.; Sah, D.K.; Yoon, H.J.; Park, S.C.; Jung, Y.S.; Ahn, Y.K.; Lee, K.H.; Lee, S.R. Redox Regulation of Phosphatase and Tensin Homolog by Bicarbonate and Hydrogen Peroxide: Implication of Peroxymonocarbonate in Cell Signaling. *Antioxidants* **2024**, *13*, 473. [CrossRef] [PubMed]
41. Zhou, G.; Liu, P.; Zhang, C.; Huang, Q.; Zhao, Z.; Wu, S.; Li, D.; Liu, H. HDAC2 counteracts vascular calcification by activating autophagy in chronic kidney disease. *FASEB J.* **2024**, *38*, e23470. [CrossRef] [PubMed]
42. Kwon, D.-H.; Eom, G.H.; Ko, J.H.; Shin, S.; Joung, H.; Choe, N.; Nam, Y.S.; Min, H.-K.; Kook, T.; Yoon, S.; et al. MDM2 E3 ligase-mediated ubiquitination and degradation of HDAC1 in vascular calcification. *Nat. Commun.* **2016**, *7*, 10492. [CrossRef] [PubMed]
43. Tian, W.; Singh, K.; Kajuluri, L.P.; Lu, J.; Lee, S.; Roh, K.; Nicholson, C.J.; Jiang, W.; Barnes, H.J.; Sato, T.; et al. Focal Adhesion Kinase Promotes Calcification of Vascular Smooth Muscle Cells via Regulation of Histone Deacetylase 4 and 5. *Arterioscler. Thromb. Vasc. Biol.* **2025**, *45*, e565–e583. [CrossRef] [PubMed]
44. Choe, N.; Shin, S.; Joung, H.; Ryu, J.; Kim, Y.K.; Ahn, Y.; Kook, H.; Kwon, D.H. The microRNA miR-134-5p induces calcium deposition by inhibiting histone deacetylase 5 in vascular smooth muscle cells. *J. Cell. Mol. Med.* **2020**, *24*, 10542–10550. [CrossRef] [PubMed]
45. Fu, Z.; Li, F.; Jia, L.; Su, S.; Wang, Y.; Cai, Z.; Xiang, M. Histone deacetylase 6 reduction promotes aortic valve calcification via an endoplasmic reticulum stress-mediated osteogenic pathway. *J. Thorac. Cardiovasc. Surg.* **2019**, *158*, 408–417.e2. [CrossRef] [PubMed]
46. Nomura, Y.; Nakano, M.; Woo Sung, H.; Han, M.; Pandey, D. Inhibition of HDAC6 Activity Protects Against Endothelial Dysfunction and Atherogenesis in vivo: A Role for HDAC6 Neddylation. *Front. Physiol.* **2021**, *12*, 675724. [CrossRef] [PubMed]
47. He, P.; Yu, H.; Jiang, L.; Chen, Z.; Wang, S.; Macrae, V.E.; Fu, X.; Zhu, D. Hdac9 inhibits medial artery calcification through down-regulation of Osterix. *Vasc. Pharmacol.* **2020**, *132*, 106775. [CrossRef] [PubMed]
48. Xiong, L.; Xiao, Q.; Chen, R.; Huang, L.; Gao, J.; Wang, L.; Li, G.; Li, Y. Histone deacetylase 9 promotes osteogenic trans-differentiation of vascular smooth muscle cells via ferroptosis in chronic kidney disease vascular calcification. *Ren. Fail.* **2024**, *46*, 2422435. [CrossRef] [PubMed]
49. Xiao, Y.; Awasthee, N.; Liu, Y.; Meng, C.; He, M.Y.; Hale, S.; Karki, R.; Lin, Z.; Mosterio, M.; Garcia, B.A.; et al. Discovery of a Highly Potent and Selective HDAC8 Degrader: Advancing the Functional Understanding and Therapeutic Potential of HDAC8. *J. Med. Chem.* **2024**, *67*, 12784–12806. [CrossRef] [PubMed]
50. He, D.; Ma, J.; Zhou, Z.; Qi, Y.; Lian, Y.; Wang, F.; Yin, H.; Zhang, H.; Zhang, T.; Huang, H. TET2 suppresses vascular calcification by forming an inhibitory complex with HDAC1/2 and SNIP1 independent of demethylation. *J. Clin. Investig.* **2025**, *135*, e186673. [CrossRef] [PubMed]
51. Bornes, K.E.; Moody, M.A.; Huckaba, T.M.; Benz, M.C.; McConnell, E.C.; Foroozesh, M.; Barnes, V.H.; Collins-Burow, B.M.; Burow, M.E.; Watt, T.J.; et al. Lysine deacetylase inhibitors have low selectivity in cells and exhibit predominantly off-target effects. *FEBS Open Bio* **2025**, *15*, 94–107. [CrossRef] [PubMed]

52. Furmanik, M.; Chatrou, M.; van Gorp, R.; Akbulut, A.; Willems, B.; Schmidt, H.; van Eys, G.; Bochaton-Piallat, M.-L.; Proudfoot, D.; Biessen, E.; et al. Reactive Oxygen-Forming Nox5 Links Vascular Smooth Muscle Cell Phenotypic Switching and Extracellular Vesicle-Mediated Vascular Calcification. *Circ. Res.* **2020**, *127*, 911–927. [CrossRef] [PubMed]
53. Vitale, I.; Pietrocola, F.; Guilbaud, E.; Aaronson, S.A.; Abrams, J.M.; Adam, D.; Agostini, M.; Agostinis, P.; Alnemri, E.S.; Altucci, L.; et al. Apoptotic cell death in disease—Current understanding of the NCCD 2023. *Cell Death Differ.* **2023**, *30*, 1097–1154. [CrossRef] [PubMed]
54. Pustlauk, W.; Westhoff, T.H.; Claeys, L.; Roch, T.; Geißler, S.; Babel, N. Induced osteogenic differentiation of human smooth muscle cells as a model of vascular calcification. *Sci. Rep.* **2020**, *10*, 5951. [CrossRef] [PubMed]
55. Kessler, J.R.; Bluemn, T.S.; DeCero, S.A.; Dutta, P.; Thatcher, K.; Mahnke, D.K.; Knas, M.C.; Kazik, H.B.; Menon, V.; Lincoln, J. Exploring molecular profiles of calcification in aortic vascular smooth muscle cells and aortic valvular interstitial cells. *J. Mol. Cell. Cardiol.* **2023**, *183*, 1–13. [CrossRef] [PubMed]
56. Long, K.; Close, D.A.; Johnston, P.A.; Huryn, D.M. Replacement of the hydroxamic acid group in the selective HDAC8 inhibitor PCI-34051. *Bioorganic Med. Chem. Lett.* **2024**, *108*, 129810. [CrossRef] [PubMed]

Disclaimer/Publisher's Note: The statements, opinions and data contained in all publications are solely those of the individual author(s) and contributor(s) and not of MDPI and/or the editor(s). MDPI and/or the editor(s) disclaim responsibility for any injury to people or property resulting from any ideas, methods, instructions or products referred to in the content.